JGR Earth Surface

RESEARCH ARTICLE
10.1029/2022JF006769

From Grains to Plastics: Modeling Nourishment Patterns and Hydraulic Sorting of Fluvially Transported Materials in Deltas

Kyle Wright[1], Jayaram Hariharan[1], Paola Passalacqua[1], Gerard Salter[2], and Michael P. Lamb[2]

[1]Department of Civil, Architectural, and Environmental Engineering, Center for Water and the Environment, University of Texas at Austin, Austin, TX, USA, [2]Division of Geological and Planetary Sciences, California Institute of Technology, Pasadena, CA, USA

Key Points:

- We advance a unified reduced-complexity modeling framework for simulating transport pathways of a diverse range of suspended materials
- We simulate and compare patterns of nourishment and connectivity in river deltas for a range of materials, discharge, and tidal conditions
- Differential topographic steering hydraulically sorts different kinds of materials in space, with different sensitivities to external forces

Supporting Information:

Supporting Information may be found in the online version of this article.

Correspondence to:

P. Passalacqua,
paola@austin.utexas.edu

Citation:

Wright, K., Hariharan, J., Passalacqua, P., Salter, G., & Lamb, M. P. (2022). From grains to plastics: Modeling nourishment patterns and hydraulic sorting of fluvially transported materials in deltas. *Journal of Geophysical Research: Earth Surface*, *127*, e2022JF006769. https://doi.org/10.1029/2022JF006769

Received 23 MAY 2022
Accepted 3 NOV 2022

Abstract Understanding the way fluvially transported materials are partitioned in river deltas is essential for predicting their morphological change and the fate of environmental constituents and contaminants. Translating water-based partitioning estimates into fluxes of nonwater materials is often difficult to constrain because most materials are not uniformly distributed in the water column and may have characteristic transport pathways that differ from the mean flow. Here, we present a novel reduced-complexity modeling approach for simulating the patterns of transport of a diverse range of suspended fluvial inputs influenced by vertical stratification and topographic steering. We utilize a mixed Eulerian-Lagrangian modeling approach to estimate the patterns of nourishment and connectivity in the Wax Lake and Atchafalaya Deltas in coastal Louisiana. Using the reduced-complexity particle routing model `dorado`, in conjunction with a calibrated `ANUGA` hydrodynamic model, we quantify how transport patterns in each system change as a function of a material's Rouse number and environmental conditions. We find that even small changes to local topographic steering lead to emergent system-scale changes in patterns of fluvial nourishment, with greater channel-island connectivity for positively buoyant materials than negatively buoyant materials, hydraulically sorting different materials in space. We also find that the nourishment patterns of some materials are more sensitive than others to changes in discharge, tidal conditions, and anthropogenic dredging. Our results have important implications for understanding the eco-geomorphic evolution of deltas, and our modeling framework could have interdisciplinary implications for studying the transport of materials in other systems, including sediments, nutrients, wood, plastics, and biotic materials.

Plain Language Summary River deltas are complex and important landscapes and the way they build land and function depends on how flows of water, sediment, floating vegetation, and other materials get distributed among different channels and wetlands. In addition, deltas are important destinations for pollutants of interest like plastics and oils. While we have an increasingly good understanding of how water flows through deltas, it remains hard to estimate the transport pathways of other materials suspended in the water. One important reason for this is that many materials are more or less dense than water, so they tend to concentrate either at the greatest depths (like sediments) or at the water surface (like plastics), which can affect how they flow downstream and can be hard to model in a generalizable way. In this study, we use the particle-routing model `dorado` to simulate the flows of many different kinds of materials using the same modeling framework, which we apply to two river deltas in coastal Louisiana. We compare how patterns of transport change as a function of material, discharge, and tidal conditions. We discuss how these transport patterns differ from those of water and each other, with important implications for how these landscapes evolve.

1. Introduction

The morphologies of river deltas are built by the complex feedbacks between the way fluvially transported materials get distributed throughout the delta plain and the way the resulting landforms subsequently steer flows of matter (Edmonds et al., 2021). In general, water is the driving force controlling the transport of geomorphic building blocks like sediments, nutrients, biotic materials, and other fluvial inputs throughout distributary systems. Hydrological connectivity, or the water-mediated transport of matter and energy between different landscape elements (Amoros & Bornette, 2002; Wohl et al., 2019), has been shown to be an important control on deltaic processes. In the Wax Lake Delta (WLD, Figure 1), for example, many studies have attempted to quantify the partitioning of water between distributary channels and between channels and interdistributary islands. Channel-island

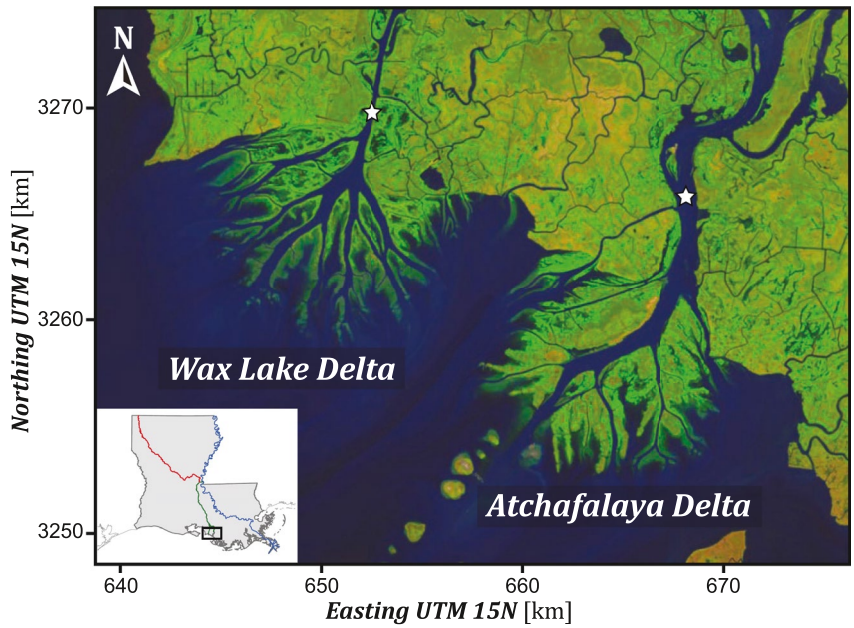

Figure 1. The Wax Lake Delta and Atchafalaya Delta distributary systems in coastal Louisiana. Apex locations used to seed particles are indicated with white stars. False color imagery taken by Landsat 9 OLI in December 2021, courtesy of USGS.

connectivity is known to be substantial in this system, with an estimated 23%–59% of the total fraction of input water flow entering interdistributary islands before being discharged into the bay (Christensen et al., 2020; Hiatt & Passalacqua, 2015, 2017; Liang, Geleynse, et al., 2015; Shaw et al., 2016). Connectivity is thought to increase during the flood season, but is present even at low-to-median flows (Hiatt & Passalacqua, 2015), and is generally controlled by channel geometry, vegetated roughness (Hiatt & Passalacqua, 2017; Olliver & Edmonds, 2021; Olliver et al., 2020), and vegetation spatial patterns (Wright et al., 2018). This influx of water is certain to bring with it other materials that help islands aggrade and influence ecosystem function, but translating estimates of hydrological connectivity into fluxes of nonwater materials remains poorly constrained and little understood.

Generally speaking, there is good reason to suspect that the transport patterns of other materials might differ from that of water. For example, most fluvially transported materials tend to have nonuniform concentration-depth profiles due to vertical stratification. Because light and heavy materials tend to concentrate at different heights in the water column (Brush & Lucien, 1965; De Leeuw et al., 2020; Repasch et al., 2022; Slingerland, 1984), this implies that some materials may be more sensitive than others to topographic steering at bifurcations (Edmonds & Slingerland, 2008) or more likely to overtop submerged island levees. This "hydraulic sorting" mechanism may create asymmetries in the way water and geomorphic building blocks like sediment and biota (seeds, floating vegetation, and large wood) are partitioned within distributary networks (e.g., Wagner & Mohrig, 2019) and between channels and interdistributary islands, leading to differential patterns in their deposits. Persistent spatial gradients between sediment and biotic materials could influence system processes, including vegetation colonization (Chambert & James, 2009), channel migration and reorganization (Lauzon & Murray, 2022), island aggradation (Ma et al., 2018; Wagner et al., 2017), and patterns of water and sediment connectivity (Hiatt & Passalacqua, 2015; Olliver & Edmonds, 2021). In addition to these core building blocks for deltaic deposits, many other fluvially transported materials of scientific interest make their way through river deltas. Some of these materials may affect deltaic morphology, such as ice (Forbes & Taylor, 1994; Lauzon et al., 2019; Piliouras et al., 2021) or nutrients (Hiatt et al., 2018; Knights et al., 2020), but many others are of interest for reasons relating to contaminant fate and transport (Atwood et al., 2019; Lebreton et al., 2017), ecology (Glenn et al., 2001), or carbon budgeting (Repasch et al., 2022; Shields et al., 2017; Torres et al., 2020).

Very little is known about how these other materials are partitioned through river deltas because it can be hard to quantify magnitudes of nonwater fluxes. These estimates rely on first developing accurate water budgets, which require either extensive field campaigns (e.g., Dong et al., 2020; Hiatt & Passalacqua, 2015), well-calibrated hydrodynamic models (e.g., de Brye et al., 2011; Hiatt, 2016; Sassi et al., 2011), or remote-sensing based proxy

estimates (e.g., Dong et al., 2020). These water budgets can be a challenge on their own, particularly due to changes in discharge associated with short-term environmental conditions or long-term flux reorganization (Edmonds & Slingerland, 2008). Furthermore, it can be difficult to quantify fluxes of near-bed materials because those areas are less accessible with typical remote sensing or field-based measurements (Dong et al., 2020), and some materials are transported too infrequently to obtain good estimates of their magnitude. Due to the absence of this information, many studies either assume that nonwater fluxes are proportional to water partitioning (e.g., Whaling & Shaw, 2020) or assume that observations from the uppermost section of the water column are applicable over the full depth (e.g., Atwood et al., 2019; Jensen et al., 2019; Walker & Hammack, 2000; Van Sebille et al., 2020), the accuracy of which is uncertain. Numerical modeling has proven to be a useful approach to fill in these knowledge gaps. Many studies have applied morphodynamic models to deltaic settings to quantify the partitioning of sediments in distributary networks (e.g., Edmonds & Slingerland, 2008; Hanegan & Georgiou, 2015; Olliver & Edmonds, 2021; Olliver et al., 2020). Other models have been developed to study the transport of drifters like wood (Persi et al., 2019; Mazzorana et al., 2011), oils (Dagestad et al., 2018; Röhrs et al., 2018), and plastics (Atwood et al., 2019), although very few of these models have been applied specifically to deltaic environments. However, none of these models are applicable to all fluvial materials, and comparing material transport between models is likely influenced by differences in modeling choices and assumptions (Baar et al., 2019). This makes it hard to assess the accuracy of using water partitioning as a proxy for nonwater materials in a generalizable way.

In the present study, we model the first-order spatial patterns of deltaic nourishment for a wide range of fluvially transported materials influenced by differential topographic steering. We utilize a reduced-complexity approach inspired by the cellular morphodynamic model `DeltaRCM` (Liang, Voller, & Paola, 2015; Moodie et al., 2021) to model multiple materials within a single modeling framework, adapted into a mixed Eulerian-Lagrangian approach using the passive particle tracking model `dorado` (Hariharan et al., 2020). First, we summarize background information on the causes of hydraulic sorting and our modeling methodology. We then use `dorado` to compare the patterns of transport and connectivity for a variety of fluvially transported materials in the WLD and Atchafalaya Delta (ATD) systems in coastal Louisiana, USA. We perform particle-tracking simulations on top of hydrodynamic simulations that together span a range of material parameters, discharge, and tidal conditions, in order to compare the partitioning of fluxes and connectivity through each delta complex. We develop a simple conceptual model to map from the material parameters used in `DeltaRCM` and `dorado` to physical properties of materials based on Rouse sediment-suspension theory. Finally, we discuss how these results fit together with prior research in the Atchafalaya region.

2. Background

2.1. Vertical Stratification, Topographic Steering, and Hydraulic Sorting

All materials that are positively or negatively buoyant in water are subject to local stratification in the water column, leading to a nonuniform concentration profile with depth. It has been understood for many decades that this process can lead to the segregation or "sorting" of sediments by grain size during hydraulic transport (Brush & Lucien, 1965; Slingerland, 1984), especially in combination with differential entrainment and granular sorting processes. The vertical stratification of particulates can be described as a balance between gravitational settling and turbulent mixing (Van Rijn et al., 1993), and the shape of the resulting concentration profile is often described using Rouse-Vanoni theory (Rouse, 1937; Vanoni, 1946). A simplified 1-D model for this can be written as a diffusion equation using Fick's law as follows:

$$\omega_s C(z) + \varepsilon_s \frac{\partial C(z)}{\partial z} = 0 \tag{1}$$

in which ω_s is the particle settling velocity (which can be negative), $C(z)$ is the concentration at height z above the bed, and ε_s is the eddy diffusivity or mixing coefficient. Choices for the functional form of ε_s vary in the literature depending on the application, but two common forms that have been used assume that it is either (a) constant over the full depth or (b) parabolic with the highest mixing at half the water depth (Van Rijn et al., 1993). Each of these choices leads to a different solution to this equation, which can be written as follows:

$$C_0(z) = C_a \exp\left(-\frac{\alpha R[z-a]}{h}\right) \tag{2}$$

$$C_2(z) = C_a\left(\frac{h-z}{z}\frac{a}{h-a}\right)^R \tag{3}$$

in which h is the water depth, C_a is the reference concentration at some height a, and the coefficient $\alpha \approx 6$. The Rouse or suspension number is defined as $R = \omega_s/\beta\kappa u_*$, in which u_* is the shear velocity, $\kappa \approx 0.41$ is the von Kármán constant, and β is a dimensionless coefficient that accounts for differences in the diffusivity of momentum and sediment, which we assume to be unity. The indices 0 and 2 indicate the Rouse profiles derived using the 0th-order (constant) and 2nd-order (parabolic) diffusivity, respectively.

It is worth noting that each of these equations (and their underlying assumptions) are symmetric about the z-axis and can describe negatively and positively buoyant materials alike. Rouse profiles have been used extensively to describe the concentration of negatively buoyant sediment grains (e.g., Camenen & Larson, 2008; De Leeuw et al., 2020; Esposito et al., 2017; Lamb et al., 2008, 2020; Van Rijn et al., 1993). Likewise, similar or identical models have been derived for the concentration profiles of positively buoyant materials, including oil (Röhrs et al., 2018), fish eggs (Sundby, 1983), frazil ice (Svensson & Omstedt, 1998), and plastic debris (Cowger et al., 2021; Kooi et al., 2016; Kukulka et al., 2012; Waldschläger et al., 2022). Traditionally the power-law model has been more common in sediment transport applications and the exponential model more common for use with floating materials in the marine environment, but in each case there have been exceptions (e.g., Camenen & Larson, 2008; Cowger et al., 2021). Regardless of whether the exponential or power-law form of the model is chosen, the shape of the resulting concentration profile is similar.

In river deltaic settings, fluvial inputs of any of the aforementioned materials may be scientifically relevant. Aside from sediments, other common types of negatively buoyant materials may include biogenic particulate organic carbon or POC (Bouchez et al., 2014; Repasch et al., 2022), dense large wood (Wohl, 2013), some plastics (Cowger et al., 2021; Kane & Clare, 2019; Waldschläger et al., 2022), and smaller particulates that have flocculated into larger aggregates (Lamb et al., 2020). Because these materials concentrate near the bed, their transport is more sensitive to topographic steering at bifurcations (Edmonds & Slingerland, 2008) and more inclined to follow topographic lows in the landscape (Liang, Voller, & Paola, 2015), leading to higher concentrations in the channel thalweg (DuMars, 2002). Positively buoyant materials, on the other hand, are relatively shielded from the influence of the bed and would have a greater propensity than sinking materials to overtop submerged channel levees. In addition, due to environmental effects like wind and waves, buoyant materials likely have increased dispersion in their flow paths relative to the mean flux of water (Reed et al., 1994), which also suggests that changing environmental conditions may not affect the transport trajectories of all types of materials equally. Common types of positively buoyant materials in river deltas can include macroalgae (Messyasz et al., 2018; Thiel & Gutow, 2004), light large wood (Le Lay et al., 2013; Wohl, 2013), mineral and biogenic oils (Ayoub et al., 2018; Cathcart et al., 2020; De Laurentiis et al., 2020; Reed et al., 1994; Röhrs et al., 2018; Shaw et al., 2016), many juvenile organisms (e.g., seeds, larvae, and eggs) (Chambert & James, 2009; Sundby, 1983; Thiel & Gutow, 2005), frazil ice (Svensson & Omstedt, 1998), most plastics (Atwood et al., 2019; Lebreton et al., 2017; Van Sebille et al., 2020), and floating vascular vegetation (Thiel & Gutow, 2004).

The relevant idea to underscore here is that vertical segregation of material in the water column, when combined with topographic steering, can subsequently influence horizontal transport (Chambert & James, 2009; Repasch et al., 2022; Slingerland, 1984). Particulates concentrated near the top or bottom of the water column have a different relative likelihood to make the jump over obstacles in the flow path, such as submerged levees or vegetation (Figure 2), resulting in different patterns of connectivity. In river deltas with very small water surface gradients, $\nabla\eta \approx \mathcal{O}\left(10^{-5}\right)$, hydraulic sorting may be a particularly important control on the resulting material deposits.

2.2. The Reduced-Complexity Approach of `DeltaRCM`

Even though all fluvial inputs are subject to many of the same physical processes during transport, numerical models are rarely designed to handle more than one category of material at a time. Additionally, most large-scale model applications rely on implementations of the depth-averaged (2D) shallow water equations due to their good performance and ease of implementation, which makes it challenging to simulate the (ostensibly 3D) transport processes directly.

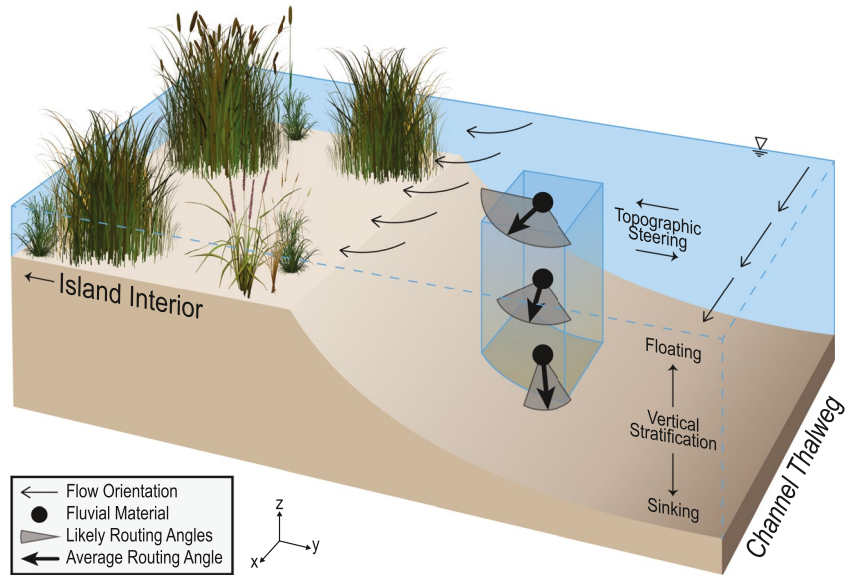

Figure 2. Conceptual schematic demonstrating the connection between vertical stratification, topographic steering, and the resulting sorting of materials in space. Particles of different buoyancy are shown at three different heights in the water column (vertical stratification), which leads to a different influence of topographic gradients and barriers on horizontal transport (topographic steering), as indicated by differences in the routing angles. In this schematic, positively buoyant particles are more likely to overtop the submerged island levee and enter the island interior, whereas negatively buoyant particles are more likely to concentrate near the channel thalweg.

One possibility is to make use of a reduced-complexity approach, in which the complex physics of all of these materials can be simplified into a single rule-based framework. This is the approach used by the cellular morphodynamic model `DeltaRCM` (Liang, Voller, & Paola, 2015; Moodie et al., 2021), which routes water and two types of sediment using similar transport rules. Aside from the morphodynamic component that deposits/reentrains sediment, the only difference in the way `DeltaRCM` routes water, mud, and sand is the choice of a parameter, θ, which represents the strength of topographic steering on parcels of each material. Numerous studies have shown that `DeltaRCM` successfully builds realistic deltas despite its simplified physics (Liang, Voller, & Paola, 2015, Liang, Van Dyk, & Passalacqua, 2016), and various versions of it have been used to model delta morphodynamics under the influence of vegetation (Lauzon & Murray, 2018, 2022), permafrost (Lauzon et al., 2019; Piliouras et al., 2021), and subsidence (Liang, Kim, & Passalacqua, 2016; Moodie & Passalacqua, 2021). `FlowRCM` (the water routing module of the code) has been tested against full-physics hydrodynamic models like `Delft3D`, and has been shown to accurately reproduce flux partitioning and connectivity in the WLD to within a few percent (Liang, Geleynse, et al., 2015).

2.3. Passive Lagrangian Particle Transport With `dorado`

Recently, the same random walk methodology of `DeltaRCM` was adopted and repackaged into the fully passive Lagrangian particle-routing model `dorado` for use with flow fields from more accurate full-scale hydrodynamic models (Hariharan et al., 2020). `dorado`'s mixed Eulerian-Lagrangian approach has multiple advantages. First, the use of more physics-based hydrodynamic flow fields likely further reduces the errors that do exist in FlowRCM, including issues reproducing realistic water surface elevations and gradients (Liang, Geleynse, et al., 2015). Second, it allows for the transport rules of `DeltaRCM` to be directly applied to models of real landscapes. Finally, the Lagrangian framework is ideal for studying patterns and timescales of material transport (Doyle & Ensign, 2009) compared to more traditional Eulerian models, and the mixed approach achieves this without sacrificing the accuracy and computational efficiency of the Eulerian model. `dorado` has been successfully used to study the timescales of fluvial transport in river-floodplain systems (Tull et al., 2022) but has yet to be used to analyze spatial patterns of transport for different materials.

`dorado` utilizes a weighted random walk methodology (Pearson, 1905) to route passive particles in a Lagrangian framework, in which transport of particles (or parcels) is modeled as a stochastic Markovian process.

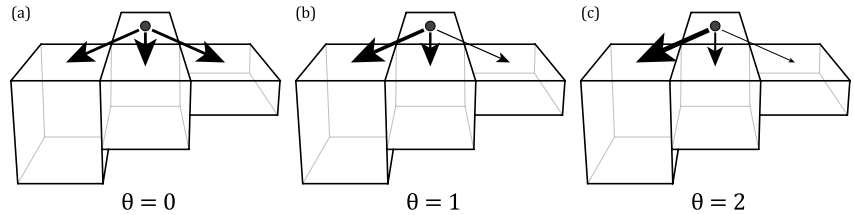

Figure 3. Influence of `dorado`'s θ parameter on downstream routing weights. (a) If $\theta = 0$, the depth of downstream cells has no influence on routing weights. (b) If $\theta = 1$, routing weights are linearly sensitive to depth. (c) If $\theta > 1$, routing weights are nonlinearly sensitive to depth.

Particles are routed on a Cartesian grid using the eight-neighbor "D8" method (O'Callaghan & Mark, 1984), with a physics-based reduced-complexity approach similar to other agent-based or cellular models (Doyle & Ensign, 2009; Mazzorana et al., 2011; Murray & Paola, 2003). At each step, the local routing weights in each direction are computed as a function of flow inertial components and the water surface gradient, using the same methodology as `DeltaRCM`. Here, we provide a brief overview of this methodology, but more thorough descriptions can be found in Hariharan et al. (2020) and the `dorado` documentation, as well as in Liang, Voller, and Paola (2015).

Each particle's local routing weights are sensitive to the choice of two global parameters: γ and θ. The γ parameter is used to compute the unit vector of the downstream flow direction $\widehat{\mathbf{F}}$, based on the inertial and surface gradient components from a hydrodynamic flow field, using the following equation:

$$\mathbf{F} = \gamma\left(\widehat{\nabla\boldsymbol{\eta}}\right) + (1-\gamma)\widehat{\mathbf{q}_\mathbf{w}} \tag{4}$$

in which $\widehat{\nabla\boldsymbol{\eta}}$ and $\widehat{\mathbf{q}_\mathbf{w}}$ represent unit vectors for the surface gradient and inertial components, respectively, γ is a constant $\in [0, 1]$, and $\widehat{\mathbf{F}} = \mathbf{F}/|\mathbf{F}|$. In `DeltaRCM`, larger γ values increase downslope relaxation of the water surface in the numerical solution, which increases diffusivity in the flow field (Liang, Voller, & Paola, 2015). However, because `dorado` uses flow fields from more accurate physics-based hydrodynamic models, it is appropriate to choose a $\gamma \leq 0.05$ to give more credence to the inertial components, which more accurately align with the orientation of fluxes.

After the downstream flow direction has been set by accounting for inertia, we then compute the relative routing weights, w_i, to each of the neighboring cells. The θ parameter controls the dependence of these routing weights on the water depths, h_i, of each neighboring cell, according to the following equation:

$$w_i = \frac{h_i^\theta}{\Delta_i}\max\left(0, \widehat{\mathbf{F}}\cdot\widehat{\mathbf{d}_\mathbf{i}}\right) \tag{5}$$

in which $\widehat{\mathbf{d}_\mathbf{i}}$ is the unit vector pointing in the direction of cell i, and Δ_i is the D8 cellular distance. In this formulation, the flow depth h_i plays the role of a resistance term, whereby shallower depths have a greater resistance and are therefore likely to receive a smaller fraction of the flow (Liang, Voller, & Paola, 2015). Alternatively, an equally valid description of this framework is that material routes from one cell to its downstream neighbors in proportion to their flow depth (modulated by the exponent θ, Figure 3). In the case of $\theta = 1$, which is the neutral setting used for water in `DeltaRCM`, this is a natural extension of conservation of mass: if multiple downstream cells have the same inlet velocity but different depths, the depth-integrated flux of water parcels into each must be scaled linearly to maintain their different depths (Figure 3b). In contrast, a material like coarse sediment, which tends to concentrate near the bottom of the water column, is likely more sensitive to changes in topography and more likely to follow topographic lows (Figure 3c). In `DeltaRCM`, this increased sensitivity to topographic steering is modeled with a higher value of $\theta \approx 2$ for sand transport, while the value for mud remains closer to the value for water (Liang, Voller, & Paola, 2015). One could also imagine that other secondary transport processes are embedded into this simplified framework (e.g., gravitational sliding of coarse grains downslope) which together have the net effect of increasing the fraction of material transported to the deepest downstream cells. It is worth noting here that this parameterization separating sand transport from water/mud, despite its simplicity, has proven capable of reproducing realistic patterns of sand and mud transport in deltas, as reflected

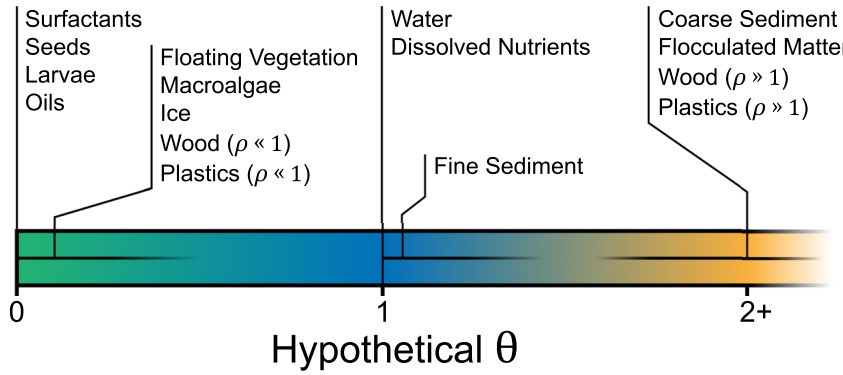

Figure 4. Hypothesized choices of θ for a range of fluvially transported materials, based on where those materials tend to concentrate in the water column (i.e., the mean elevation of their concentration-depth profile).

by the fact that `DeltaRCM` stratigraphy realistically captures multiple subsurface sand/mud distribution characteristics (Liang, Van Dyk, & Passalacqua, 2016). Furthermore, while these particles are ostensibly "passive" and do not simulate deposition or erosion, it could be just as reasonable to consider them "characteristic particles" for which deposition and erosion are always locally balanced, thereby representing a kind of "characteristic pathway" for particles in transport. This alternative conceptualization may be useful when making analogies to sediment transport theory.

3. Methods and Model Implementation

3.1. Modeling a Range of Materials With `dorado`

The present study is motivated by the key methodological insight that although water, mud, and sand were the only morphologically relevant materials considered in prior applications of `DeltaRCM` and `dorado`, there is no reason to expect that this same framework could not be applied to other fluvially transported materials. Other negatively buoyant materials aside from sand should follow similar transport physics and topographic steering with a $\theta > 1$. Likewise, at the other end of this spectrum, positively buoyant materials which travel near the water surface are likely less impacted by changes in the underlying bathymetry, and due to wind/waves could have more diffusive travel paths compared to the rest of the water column. These materials could be modeled using a lower $\theta < 1$ reflecting a relative indifference to changes in depth moving downstream (Figure 3a). Therefore, just by varying this simple θ parameter, we argue that at least the first-order transport physics of numerous different materials can be modeled using `dorado`. A nonexhaustive list of fluvially transported materials of interest and their hypothesized θ value is shown in Figure 4. Note that several of these materials could reasonably exist in multiple locations along this spectrum depending on their precise material properties—wood and plastic, for example, can be positively or negatively buoyant depending on the context (Cowger et al., 2021; Lenaker et al., 2019; Wohl, 2013).

In this study, we perform a suite of simulations to probe the impact of θ—and therefore the combined effects of stratification and topographic steering—on global patterns of transport in river deltas. While there are several caveats relating to this reduced-complexity approach, one of the many strengths of `dorado` is that we can approximate the first-order transport physics of many different materials using a single model and can therefore analyze these patterns of nourishment and partitioning without needing to worry about different modeling choices or frameworks for different materials.

3.2. Study Site: Wax Lake and Atchafalaya Deltas

In this study, we choose to focus on the Wax Lake and Atchafalaya Deltas (Figure 1), which are two small actively aggrading distributaries of the larger Mississippi River in coastal Louisiana, USA We choose these deltas because they have been the subject of substantial scientific inquiry for half a century, which provides a large amount of contextual and validation information for our analysis. Approximately 30% of the flow from the Mississippi river is diverted into the Atchafalaya River by the Old River Control structure, which then feeds each of these

distributary systems (Roberts et al., 2003). Together, these two deltas discharge approximately 238 Gt of water and 48.4 Mt of sediment into the Gulf of Mexico each year, with approximately 43% of it being through the WLD and the remaining fraction through the ATD (Allison et al., 2012). These deltas have built approximately 85 ± 44 km^2 of new subaerial land since 1973 (Zhang et al., 2021), in addition to substantial subaqueous deposits (Shaw et al., 2018), making the Atchafalaya distributary watershed one of the only regions of Louisiana's coast that is not losing land (Couvillion et al., 2017).

Most prior studies of this system have focused on the WLD due to its relative lack of anthropogenic influence. Aside from a small portion of Campground Pass which is occasionally dredged, the majority of WLD has evolved naturally, for which many have deemed it a natural prototype for possible future engineered sediment diversion projects along the Mississippi River (Kim et al., 2009; Paola et al., 2011). In contrast, the ATD is regularly dredged for shipping purposes out to the continental shelf, and the resulting dredge spoil deposits have left a visible signature on the structure of the landscape (Zhang et al., 2021). Both deltas are considered discharge-dominated, with a microtidal amplitude of ≈25 cm. Vegetation in these deltas is strongly correlated with topography, with distinct species clustered into subtidal, intertidal, and supratidal communities (Bevington & Twilley, 2018; Carle et al., 2014; Ma et al., 2018).

The WLD and ATD are the destination of many of the aforementioned types of fluvially transported materials (Figure 4). Among these inputs, the most studied are unsurprisingly water and sediment. Our understanding of water flow patterns and partitioning in the WLD has improved significantly in recent years thanks to extensive field campaigns using Acousting Doppler Current Profilers (ADCPs) (Hiatt, 2016; Hiatt & Passalacqua, 2015), remote sensing analyses using spectral or SAR imagery (Ayoub et al., 2018; Salter et al., 2022; Shaw et al., 2016), and hydrodynamic modeling approaches (Christensen et al., 2020; Liang, Geleynse, et al., 2015; Hiatt & Passalacqua, 2017; Hiatt et al., 2018). More recent studies have begun to tease apart the interplay between hydrological and sediment connectivity in the WLD using morphodynamic models (Olliver & Edmonds, 2021; Olliver et al., 2020), although these studies mostly focused on fine silt, which is less likely to exhibit significant vertical stratification. Floating vegetation is a common sight in the WLD, in which the invasive *Eichhornia crassipes* (water hyacinth) can be found floating downstream, and typically forms large floating mats in the island interiors and along channel margins (Carle et al., 2014; Ma et al., 2018). Aerial imagery of the WLD often shows visible streaklines indicating biogenic oils and organic matter on the water surface (Ayoub et al., 2018; Cathcart et al., 2020; De Laurentiis et al., 2020; Shaw et al., 2016). Several prior studies have investigated the transport and storage of nutrients such as Nitrogen and Carbon in the WLD (Christensen et al., 2020; Hiatt et al., 2018; Knights et al., 2020; Shields et al., 2017). And finally, field experience has shown that large wood and plastic debris can usually be found deposited along island levees in the WLD, although we are unaware of any attempts to quantify the magnitude of these deposits. Due to this accumulation of data and evidence, we believe the WLD and ATD are the ideal location in which to test transport patterns for a variety of materials.

3.3. Hydrodynamic Modeling With ANUGA

For hydrodynamic modeling, we use a preexisting ANUGA model of the combined WLD/ATD system from Wright et al. (2022). ANUGA is an open-source Python-based finite volume model that solves the depth-integrated shallow water equations, using variable time-stepping on an unstructured triangular grid (Roberts et al., 2015). The software was developed for coastal applications and performs well against a number of analytic test cases (Davies & Roberts, 2015; Mungkasi & Roberts, 2013; Nielsen et al., 2005). Note that the numerical solution of ANUGA is 2D and cannot explicitly resolve 3D flow structures—rather, the implementation of dorado "adds back in" some of these vertical processes onto our 2D solution. Depth-averaged models have performed well in numerous prior studies of the WLD (Christensen et al., 2020; Hanegan & Georgiou, 2015; Hiatt & Passalacqua, 2017; Olliver et al., 2020), and flow fields from ANUGA were also used as the foundation for dorado simulations in Tull et al. (2022).

The ANUGA model from Wright et al. (2022) used a spatially variable mesh resolution that was locally refined using optical and SAR imagery to highlight hydrodynamically active regions in high resolution, with lower resolutions elsewhere to save on computational expense. A grid spacing of ≈25 m was used in hydrodynamically active areas, which included nearly all of the WLD and most of the ATD. Discharge and tidal boundary conditions were based on data from four USGS gauges and one NOAA gauge, respectively. Model bathymetry was based on a preexisting 10 m DEM mosaic which merged optical and sonar data from multiple sources (Denbina

et al., 2020). Friction was implemented in three open-water classes and three vegetation classes corresponding to subtidal, intertidal, and supratidal communities. We designed simulations to recreate the conditions in October 2016 to align with the Pre-Delta-X remote sensing and field campaign (JPL, 2021), and the model was calibrated and validated against 40 in situ water level gauges, remotely sensed water level measurements from lidar, and InSAR-derived water level change measurements within inundated wetlands (Wright et al., 2022). The model performed well against these benchmark data sets, and particularly well within the modern deposits/channel network of each delta, where we choose to focus the present study.

3.4. Simulation Design

We performed a suite of simulations to test the influence of θ, discharge, and tidal conditions on material transport in the WLD and ATD. We modeled changes to environmental conditions by modifying the boundary conditions of our `ANUGA` model. We modeled two discharge regimes, high (Q_H) and low (Q_L), which we chose to match recent values during the flood and nonflood seasons respectively. The combined inlet discharge between the two rivers in these scenarios were 3,790 m^3/s for Q_L and 14,770 m^3/s for Q_H, with a roughly 43%/57% split in flow between the WLD/ATD. About 7% of this flow exits out of two outlets in the Gulf Intracoastal Waterway to the east and west before reaching the modern delta deposits (Swarzenski, 2003). To investigate the influence of tides, we modeled both steady and unsteady tidal regimes. In the steady case, the tidal boundary was a stable Dirichlet boundary with a water surface elevation of 0.26 m NAVD88. In the unsteady case, we enforced an artificial tidal signal at the downstream boundary, which was a cosine with an amplitude of 0.25 m, a period of 24 hr, and mean elevation of 0.26 m NAVD88. We chose these values to be qualitatively similar to the diurnal tidal signal measured at the NOAA Amerada Pass station in the ATD, but without extra harmonics. Due to `ANUGA`'s inability to model waves and the computational expense of modeling wind, we neglected these environmental forcings for the purposes of this study.

We used a yieldstep of 15 min for our `ANUGA` simulations, which is the time interval at which flow fields were stored into the saved output file. For steady simulations, the model ran for 3 days to ensure the flow had stabilized, and we used the flow fields from the last time step as our `dorado` input. For unsteady simulations, we gave the model a full 7 days to stabilize the tidal signal, and we used flow fields from the last day of the simulation as our `dorado` input. Because the hydrodynamic solution is cyclical with a diurnal period, we looped the flow fields from the last day of the simulation for the duration of an unsteady `dorado` simulation. We resampled all `ANUGA` flow fields to a 25 m uniform Cartesian grid (which is required for `dorado`) using `dorado`'s built-in inverse-distance-weighted interpolation function using three nearest-neighbors, and cropped to the bounding box given by UTM 15N coordinates [639000, 671900, 3245000, 3278800].

Particles were seeded upstream of the apex of the WLD and ATD in two parallel injections, at coordinates (652570, 3270230) for the WLD and (667650, 3266400) for the ATD. In order to ensure that our results were not influenced by the time of injection relative to the tidal cycle, we seeded particles in batches over the course of one full tidal period, with 250 particles released per batch every 15 min to correspond with the `ANUGA` yieldstep. In total, 24,000 particles were seeded in each delta over the course of the first day of simulation for all simulations, and then allowed to propagate for 7 days, which was enough time for virtually all particles to exit the deltas in all but two scenarios (which were given more time). Unsteady flow fields were also updated every 15 min.

In order to approximate the dynamics of a range of materials, we routed particles using five values of $\theta \in [0, 0.5, 1, 1.5, 2]$ for each of our four model scenarios, resulting in 20 simulations in total. We implemented a $\gamma = 0$ and a `dorado` "dry depth" of 1 cm (Hariharan et al., 2020). For simplicity, we also assumed that all particles travel at the same velocity as the depth-integrated water velocity, which is a safe approximation for neutrally and positively buoyant materials (Mazzorana et al., 2011) but may become slightly less accurate as θ increases beyond 1.

3.5. Quantifying Fluvial Nourishment

In order to compare the patterns of transport between scenarios, we borrow the idea of a distributary "nourishment area," which Edmonds et al. (2011) defined as the delta area nourished by sediment passing through a given location in the system. Nourishment can be considered the deltaic analog for the contributing area in upstream channel networks (Edmonds et al., 2011; Shaw et al., 2016). However, we make two modifications to this concept for the present study. First, we extend the nourishment area concept to apply to all fluvially transported materials,

not exclusively sediment. Second, we attempt to quantify the *magnitude* of nourishment for each location in the delta as the fraction of source material that passes through that location. Using this modified framework, the original definition can be recovered as the subset of all locations in the domain through which a nonzero amount of material was transported.

To compute global nourishment estimates for each of our `dorado` simulations, we extracted from each particle's travel history the number of occasions that each cell was visited by that particle, summed across all particles in that simulation, and normalized to the range $\in [0, 1]$. The result is a system-wide map of where material is being partitioned in the delta system for some choice of θ and environmental conditions. A similar metric could be computed for specific subsections of the delta, but we chose to focus on the full delta network to get a representative temporally integrated picture for all fluvial inputs. We also applied a light Gaussian smoothing filter with a standard deviation of 0.7 to the nourishment array to reduce some of the spatial noise inherent to stochastically modeling a finite number of particles (Tull et al., 2022). Maps of nourishment were then differenced to highlight changes in transport patterns due to changes in θ, Q, or tides.

Finally, we also attempted to quantify system-wide totals for channel-island connectivity, to see how estimates of connectivity for nonwater materials might compare to those of water. We did this using pseudo-ADCP transects drawn across radial transects in the WLD at different longitudinal distances downstream, through which we measured the fractional flux of particles. This framework allowed us to more directly compare our estimates to the kinds of measurements that have been collected in the field and reported in previous literature.

4. Results

4.1. Comparing Nourishment Areas by Material

We estimated magnitudes of fluvial nourishment for each of our 20 model scenarios, and we found noteworthy differences in patterns of transport as a function of θ and environmental conditions in both the WLD (Figure 5) and the ATD (Figure 6). Across all environmental conditions, we found that increases in θ were associated with a system-wide decrease in channel-island connectivity, with greater fractions of material remaining confined to the channel network.

In the WLD, patterns of nourishment associated with the neutral case of $\theta = 1$ realistically match existing hydrological measurements collected in the field (Figures 5b, 5e, 5h and 5k). Channel-island connectivity visibly increases toward the distal portions of the delta, and the onset of channel unconfinement appears to occur in a similar location to that previously found by Hiatt and Passalacqua (2015, 2017) in low discharge conditions (Figures 5b and 5h). We measured the relative partitioning of particles among the nine largest distributaries in the WLD and compared our values to estimates from Hiatt (2016) and found very close agreement, with a mean absolute error of 1.9% and a maximum absolute error of 4.9% (Figure S1 in Supporting Information S1), which are smaller than the errors reported for FlowRCM in Liang, Geleynse, et al. (2015). The influence of a Southwest-oriented cross-flow from the Atchafalaya is visible on the Eastern side of the delta, which qualitatively matches the cross-flow visible in imagery (e.g., Figure 1). Aside from a few local variations, patterns of nourishment are fairly evenly dispersed over the whole delta front in the neutral case.

Lower values of θ (Figures 5a, 5d, 5g and 5j) show some striking differences in nourishment patterns from the neutral case. Substantial increases in the fraction of particles entering the islands were seen across all scenarios, with very little material remaining inside the distributary channels by the time flows reach the delta front. Nourishment was highest in the regions of flow convergence inside interdistributary islands, with a majority of particles exiting the delta through these locations. Interestingly, these nourishment patterns appear (at least qualitatively) identical to prior observations of biogenic streaklines visible in optical and SAR imagery (Ayoub et al., 2018; Cathcart et al., 2020; De Laurentiis et al., 2020; Shaw et al., 2016), which appears to validate the hypothesis that $\theta \approx 0$ particles behave similarly to positively buoyant materials. Compared to the neutral case, decreases in θ appear to increase nourishment in shoreline-adjacent wetlands and channels (e.g., Figures 5d, 5g and 5j).

In contrast, higher values of θ (Figures 5c, 5f, 5i and 5l) resulted in a much lower fraction of particles entering the islands than the neutral or buoyant case. Nourishment was higher inside the distributary channels across all scenarios, with most particles remaining confined all the way out to the delta front. These observations

10.1029/2022JF006769

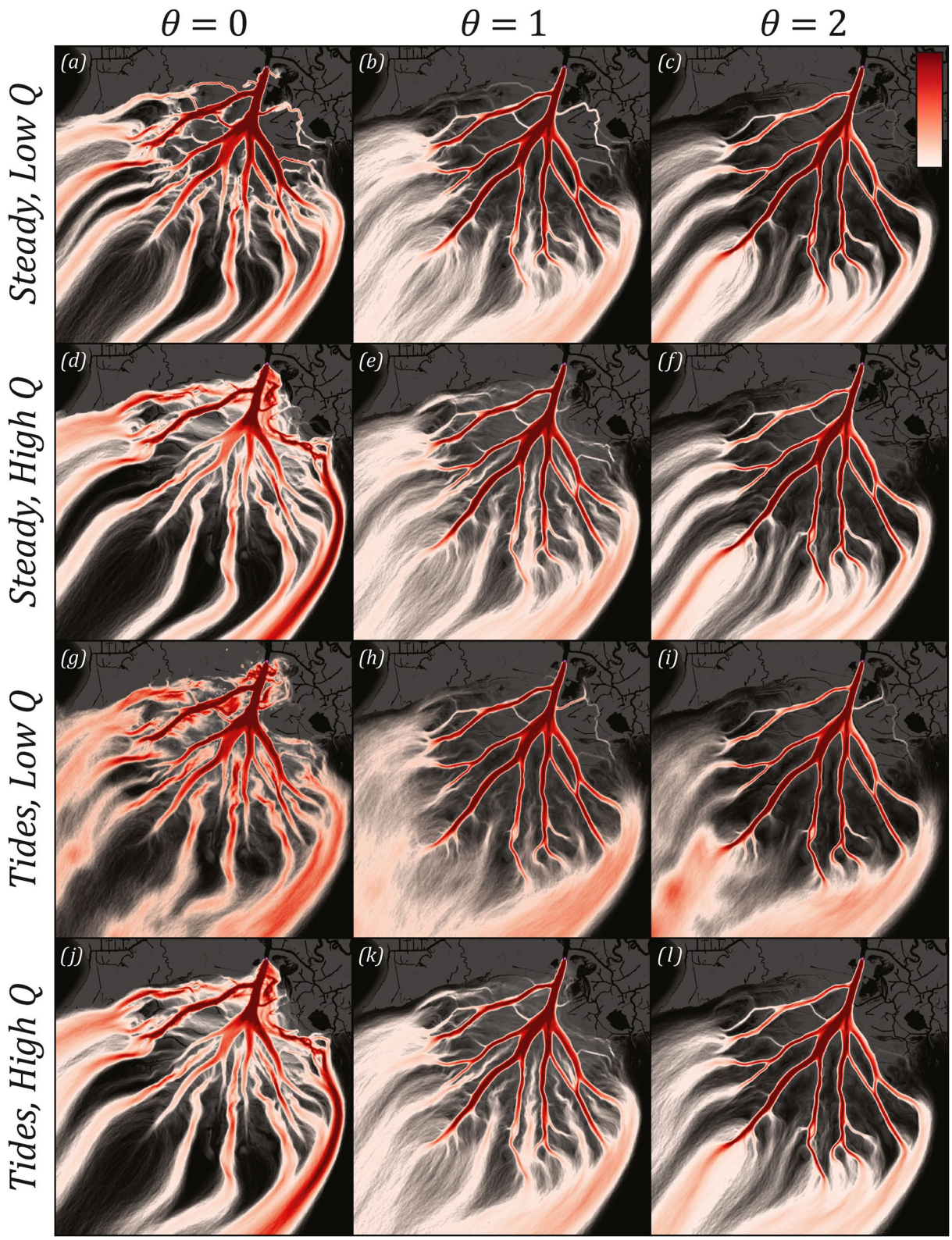

Figure 5. Magnitude of fluvial nourishment in the Wax Lake Delta for a range of environmental conditions and choices of θ. The magnitude of nourishment increases from white to red, with topography shown in the background for context. For all rows, θ increases from 0 (left) to 2 (right). The corresponding environmental conditions are, respectively (a–c) low-discharge and no tides (d–f) high-discharge and no tides (g–i) low-discharge with tides, and (j–l) high-discharge with tides.

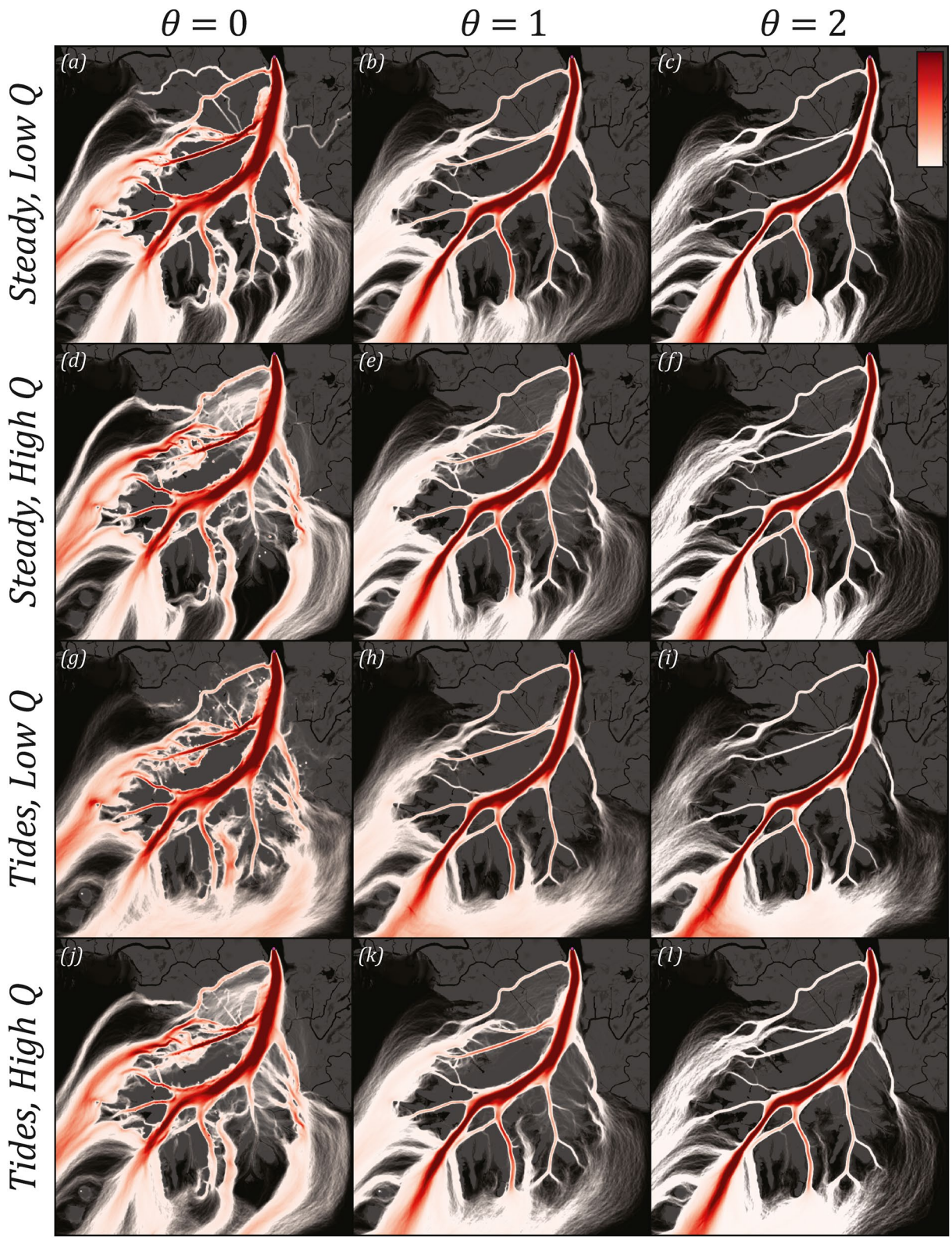

Figure 6. Magnitude of fluvial nourishment in the Atchafalaya Delta for a range of environmental conditions and choices of θ. The magnitude of nourishment increases from white to red, with topography shown in the background for context. For all rows, θ increases from 0 (left) to 2 (right). The corresponding environmental conditions are, respectively (a–c) low-discharge and no tides (d–f) high-discharge and no tides (g–i) low-discharge with tides, and (j–l) high-discharge with tides.

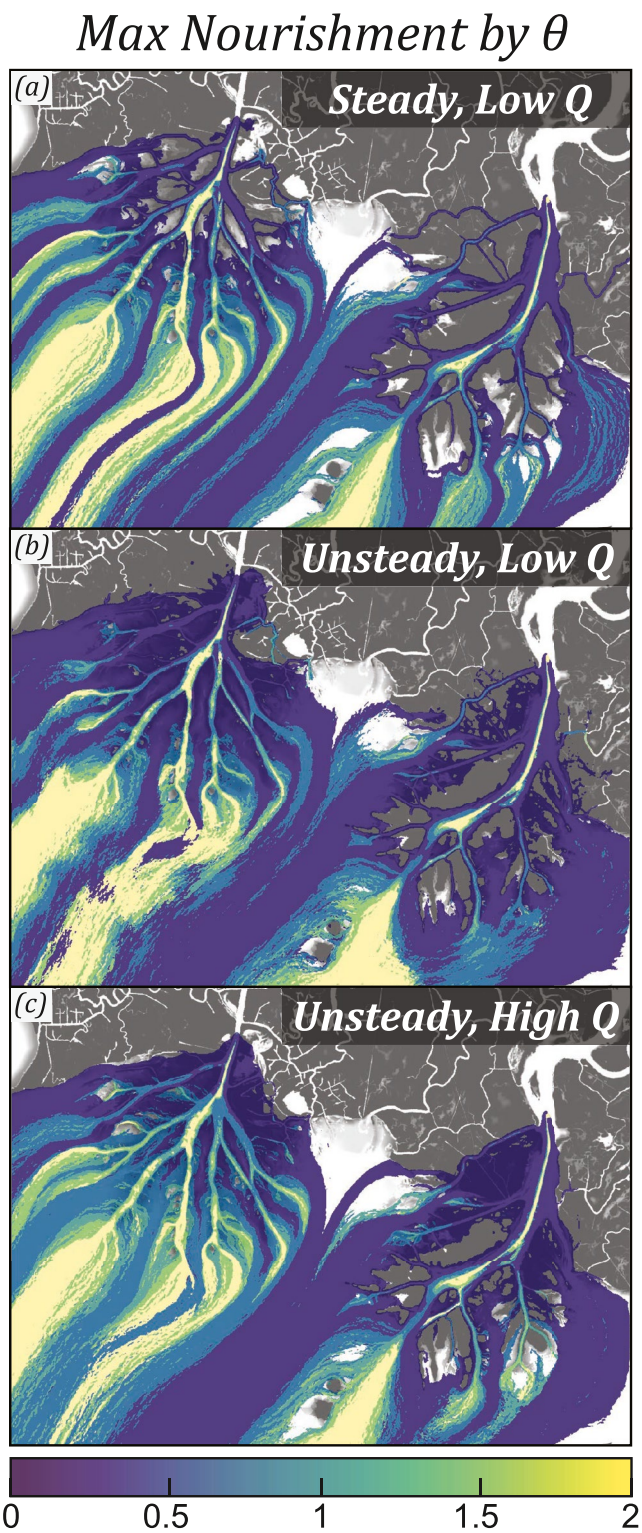

Figure 7. Choice of θ which maximized fluvial nourishment in each location, sorted by environmental conditions: (a) low-discharge and no tides; (b) low-discharge with tides; and (c) high-discharge with tides. Because tides have little influence at high-discharge, we omit the high-discharge and no tides scenario for brevity, as it looks indistinguishable from (c).

seem compatible with findings from DuMars (2002), who measured the highest sediment concentrations in the WLD over the channel thalwegs, with decreasing concentrations toward channel flanks. The only locations with visible connectivity are large secondary channels through which some particles enter the interdistributary bays, but only near the end of the subaerial extent of the islands. Due to the 25 m grid size of these simulations, which is too large to resolve some of the smaller secondary channels, this finding suggests that their absence may be an important source of error in these results, leading to underestimations in island nourishment for larger θs. Compared to lower-θ scenarios, channels in the Southeastern portion of the delta appear to be responsible for a greater discharge of these particles, particularly in Gadwall Pass.

Some of these trends visible in the WLD are also applicable to the ATD, but there are some noteworthy differences (Figure 6). Across all θs, nourishment patterns are much less diffuse in the ATD, with a majority of the particles being routed through only a few channels and a smaller degree of system-wide connectivity. The dredged Southwest Pass delivers a majority of the material to the delta front for all scenarios with a $\theta \geq 1$. Only select islands show any appreciable amount of nourishment, which likely reflects the prevalence of high-elevation dredge spoil deposits in the ATD that inhibit overbank flow along island boundaries. The flow remains relatively confined throughout the entire subaerial portion of the delta for most scenarios.

The allocated 7-day simulation run time was adequate for >99% particles to exit the domain in most scenarios. However, all runs had at least a few particles that ended up in abnormally slow-moving regions or frozen at "dead ends," that is, low-probability paths that terminated in cells that were too shallow for particles to continue forward (a few can be seen in Movie S1). Low-θ particles had a greater likelihood of finding these locations, so the fraction of frozen particles tended to increase for a decrease in θ. Two of our 20 scenarios had to be given an extra 7 days of simulation time to allow more of these frozen particles to exit the deltaic regions—specifically, both the steady and unsteady runs associated with Q_L and $\theta = 0$. While this study is not focusing on particle residence time distributions, this suggests that there may be variation in the temporal dynamics of these particles as a function of θ as well, which we would expect to be the case.

In order to quantitatively compare nourishment across all values of θ, for each grid cell in our domain, we identified the choice of θ that resulted in the greatest nourishment in that location (Figure 7), which we repeated for each environmental condition. Most of the aforementioned trends become particularly clear in this context: islands are preferentially nourished at lower values of θ, and channels are preferentially nourished at higher values of θ. However, there are some dynamics in the intermediate range of θs that are noteworthy. Many regions of the domain are maximally nourished by a choice of $\theta \approx 0.5$, particularly island topsets in high-discharge scenarios (Figure 7c). Interestingly, very few areas in either domain are maximally nourished by the neutral choice of $\theta = 1$. Because the neutral case had the most uniform patterns of nourishment over the delta front (Figures 5b, 5e, 5h and 5k), this reflects the tendency for nonwater-like materials to concentrate in particular regions of the domain. Some locations did not have any appreciable nourishment in low-forcing scenarios, which can be seen as interior "voids" in these maps (e.g., near the apex of several islands in Figure 7a). This was partly caused by simulating only a finite number of particles, but it also suggests that some parts of the system may only be receiving fluvial inputs at rare times as a

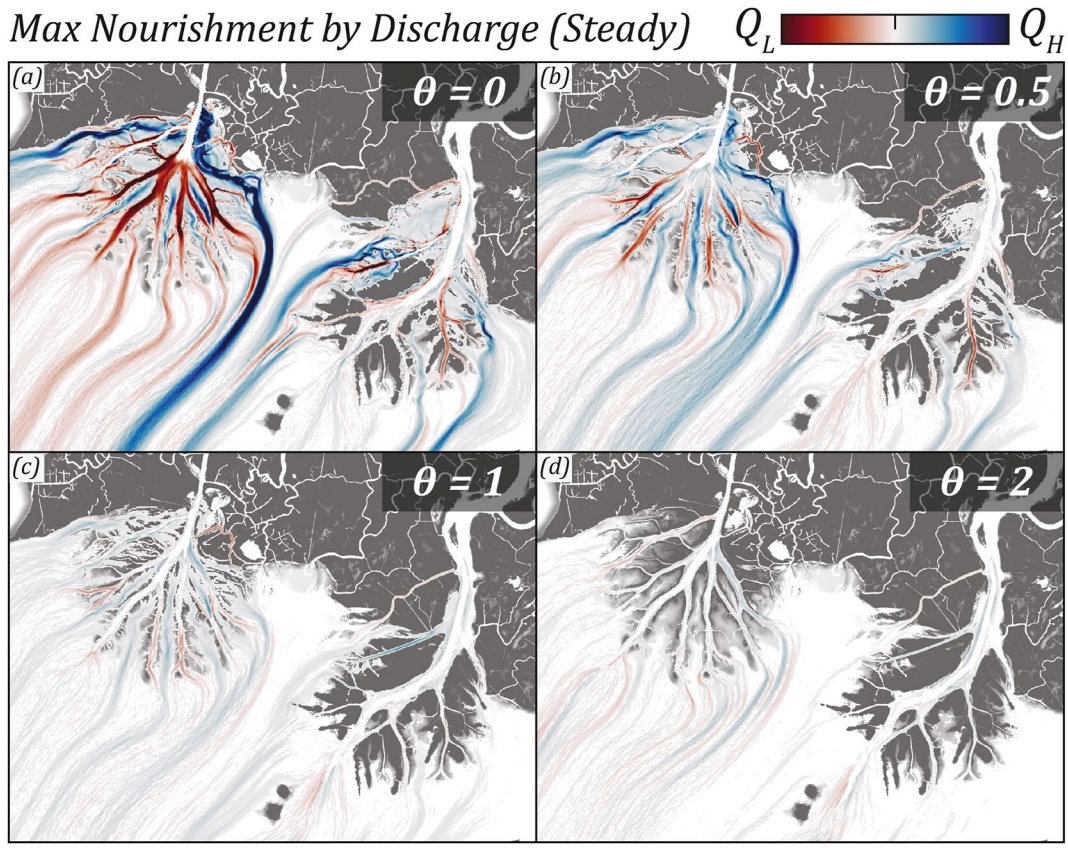

Figure 8. Choice of discharge, Q, which maximized fluvial nourishment in each location, sorted by θ. Locations with greater nourishment at Q_H are shown in blue and at Q_L are shown in red. The color-axis was truncated to changes in nourishment between −50% and +50% to better show patterns of change. Nourishment patterns show greater sensitivity to Q at low θs (a–b) than at high θs (c–d). To highlight the influence of Q, scenarios shown here neglect tides.

result of environmental conditions, which would affect their morphological evolution. In fact, the nourishment voids that are visible in the steady low-discharge scenario (Figure 7a) have considerable overlap with the regions of the WLD that Wagner et al. (2017) estimated to be no longer aggrading.

4.2. Role of External Forcings

Changes to discharge and tidal conditions clearly have a noticeable signature on nourishment dynamics. In order to isolate the influence of changing environmental conditions, we took the difference between pairs of nourishment maps as a function of either discharge (Figure 8) or tides (Figure 9). In contrast to the earlier comparison by θ (Figure 7), here there are only two possible cases (i.e., low or high forcing), which allows us to compare nourishment more quantitatively within each pairing.

Increases in discharge and tides both lead to relative increases in island nourishment. We consistently observed a greater sensitivity to environmental forcings in low-θ simulations (Figures 8a and 9a), with nourishment patterns changing very little at higher θs (Figures 8 and 9d). This finding suggests that changes to discharge and tides could have a much greater influence on the topographic steering of positively buoyant materials than other kinds of materials, likely due to the importance of even slight increases in island water surface elevations. The ATD also showed less dependence on environmental forcings than the WLD, perhaps reflecting the lesser role that those forcings had in constructing the topography of the ATD, due to widespread dredging and engineered modifications.

Increasing discharge moves the transition from confined to unconfined flow upstream, resulting in a larger fraction of flow spreading into shoreline-adjacent wetlands that are relatively inactive at low flows (Figure 8).

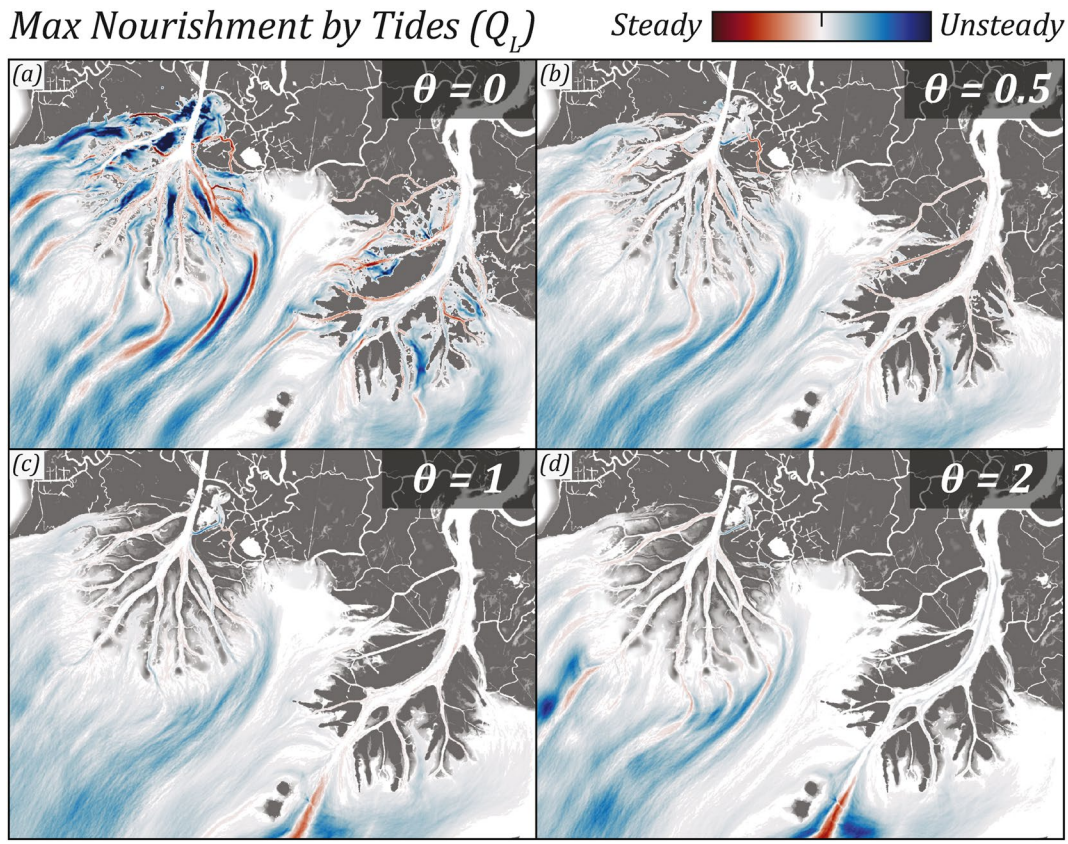

Figure 9. Choice of tidal conditions which maximized fluvial nourishment in each location, sorted by θ. Locations with greater nourishment in the unsteady case are shown in blue, with the steady case shown in red. The color-axis was truncated to changes in nourishment between −50% and +50% to better show patterns of change. Nourishment patterns show greater sensitivity to tides at low θs (a–b) than at high θs (c–d). To highlight the influence of tides, scenarios shown here correspond to low-discharge.

Channel nourishment decreases to compensate for the greater fraction of particles entering islands. Here it is important to emphasize that we are comparing *relative fractions* of nourishment that have been normalized by the incoming number of particles, not by the input mass of fluvial material.

Introducing tides also had the effect of increasing island nourishment, particularly in low-θ scenarios (Figures 9a and 9b). However, in contrast to changes in discharge, these increases in island nourishment generally did not result in a corresponding decrease in channel nourishment. This reflects the different mechanisms of connectivity in each scenario: tides nourished islands by recirculating material back upstream, whereas floods nourished islands by directly overtopping island levees. It is for this same reason that unsteady runs showed slightly greater nourishment out in the bay for all scenarios (Figure 9), where tidal reorganization led to more tortuous flow paths over the delta front.

Trends shown in Figures 8 and 9 were limited to cases where one forcing was minimized while the other was varied, in order to best observe the effect of each forcing in isolation. However, we did observe a few compounding effects worth noting. First, the importance of tidal changes was greatly diminished in the case of high-discharge due to decreases in the tidal prism, implying that tides have a lesser effect on nourishment patterns during the flood season. Second, introducing tides led to a greater increase in island nourishment than did an increase in discharge, due to the greater amount of time material spent circulating inside interdistributary bays under the influence of tides. The combination of these two trends led to a surprising and unintuitive result: in the unsteady case, increases in discharge actually resulted in decreases in (relative) island nourishment, due to the reduced tidal prism. Superimposing increases in both environmental conditions—each of which increased island nourishment on their own—was less effective at increasing island nourishment compared to tides alone.

4.3. Quantifying Connectivity

The total fraction of particles that exited the domain through each island and channel segment of our pseudo-ADCP transects (Figure 10a) varied considerably as a function of θ and discharge. We found that increases in θ typically led to increases in the channelized fraction of the flow (black circles in Figures 10b–10e) and decreases in the island fraction of the flow (white circles in Figures 10b–10e), which aligns with expectations. However, this simplified description leaves out some interesting complexity. Exit fractions in some channels are actually maximized by intermediate θs (e.g., East Pass, segment 14 in Figure 10), implying that the flux in all channels does not simply increase monotonically with θ. In addition, some shoreline-adjacent channels tend to behave more similarly to islands, showing higher exit fractions at lower values of θ (e.g., Campground Pass, segment 2). The dominance of Gadwall Pass (segment 6) is also particularly apparent in this framework, capturing up to a third of the outgoing mass in some scenarios. In contrast, most islands are responsible for a similar fraction of outgoing material.

Comparing values from the upstream and downstream transects allows us to directly quantify the decrease in the channelized fraction moving downstream. Focusing first on values for the neutral case of $\theta = 1$, we estimate that the total fraction of flow that leaked into interdistributary islands increased downstream from 6% to 25% in low-discharge conditions and from 16% to 40% in high-discharge conditions ("I" and "C" indicate island and channel totals in Figures 10b–10e, respectively). Our downstream estimates of connectivity are slightly lower but in line with prior estimates of connectivity in the WLD, which is generally estimated to be between 23% and 59%, with an average estimate around ≈45% (Christensen et al., 2020; Hiatt, 2016; Hiatt & Passalacqua, 2015; Liang, Geleynse, et al., 2015; Shaw et al., 2016). This also corroborates previous findings that connectivity increases in flood conditions but is still significant even at low flows. We found that tides, despite having noteworthy impacts on the patterns of nourishment, had little impact on the total exit fractions of islands and channels, which is also in line with findings of prior studies (Christensen et al., 2020; Hiatt, 2016).

Our estimates of connectivity changed substantially for nonneutral values of θ. For values of $\theta < 1$, the total island exit fraction increased significantly, with downstream totals ranging from 42% to 64% depending on the scenario (Figures 10c and 10e). These values are similar to the 59% estimate from Shaw et al. (2016) that was derived from measurements of surface flow, perhaps implying that surface effects contributed to the high value of that estimate. At the other end, high values of $\theta = 2$ led to much smaller total amounts of connectivity, with island fractions of only 10%–15%. Interestingly, our simulations showed that the islands receiving the greatest fraction of $\theta > 1$ particles (segments 5, 7, 9, and 11 in Figure 10) are also the islands in which Olliver and Edmonds (2021) observed the highest amounts of sediment accretion.

5. Conceptual Model Development

In order to more realistically ground our results (presented here as a function of θ), we constructed a simplified conceptual model for how θ might vary as a function of material properties. Our intended goal with this conceptual model is to aid in the interpretation of our results and to suggest a possible framework for translating materials into `dorado`'s reduced-complexity space that can be used or improved in future studies.

We first imagine that particles are situated in some cell A and have some probability of being routed to two downstream cells, B or C (Figure 11a), with a flow velocity vector equally oriented toward either cell. Note that particles usually have more than two feasible downstream cells, but here the math is simplified by comparing only two choices. Furthermore, imagine that cell B has the same water depth as cell A, whereas cell C has some smaller depth, $h_A = h_B > h_C$. Due to topographic steering, these different depths imply that the relative routing weights to each cell may be different, with $w_B \geq w_c$, with some dependence on θ as a result of Equation 5.

Here, we make several key assumptions. First, we assume the vertical distribution of material in cell A can be modeled using one of the traditional Rouse profiles described by Equation 2 or Equation 3. Second, we assume that material entering each downstream cell originates from the layer of water at the same elevation in cell A, which we adopt from the conceptual models presented in Slingerland and Smith (1998) and Han and Kim (2022). In other words, routing material to a cell shallower than cell A would be similar to *truncating* the bottom of this depth profile, diverting some of that material to cell B—the significance of which depends on the shape of the concentration profile in cell A and the relative differences in depth between cells B and C. These assumptions

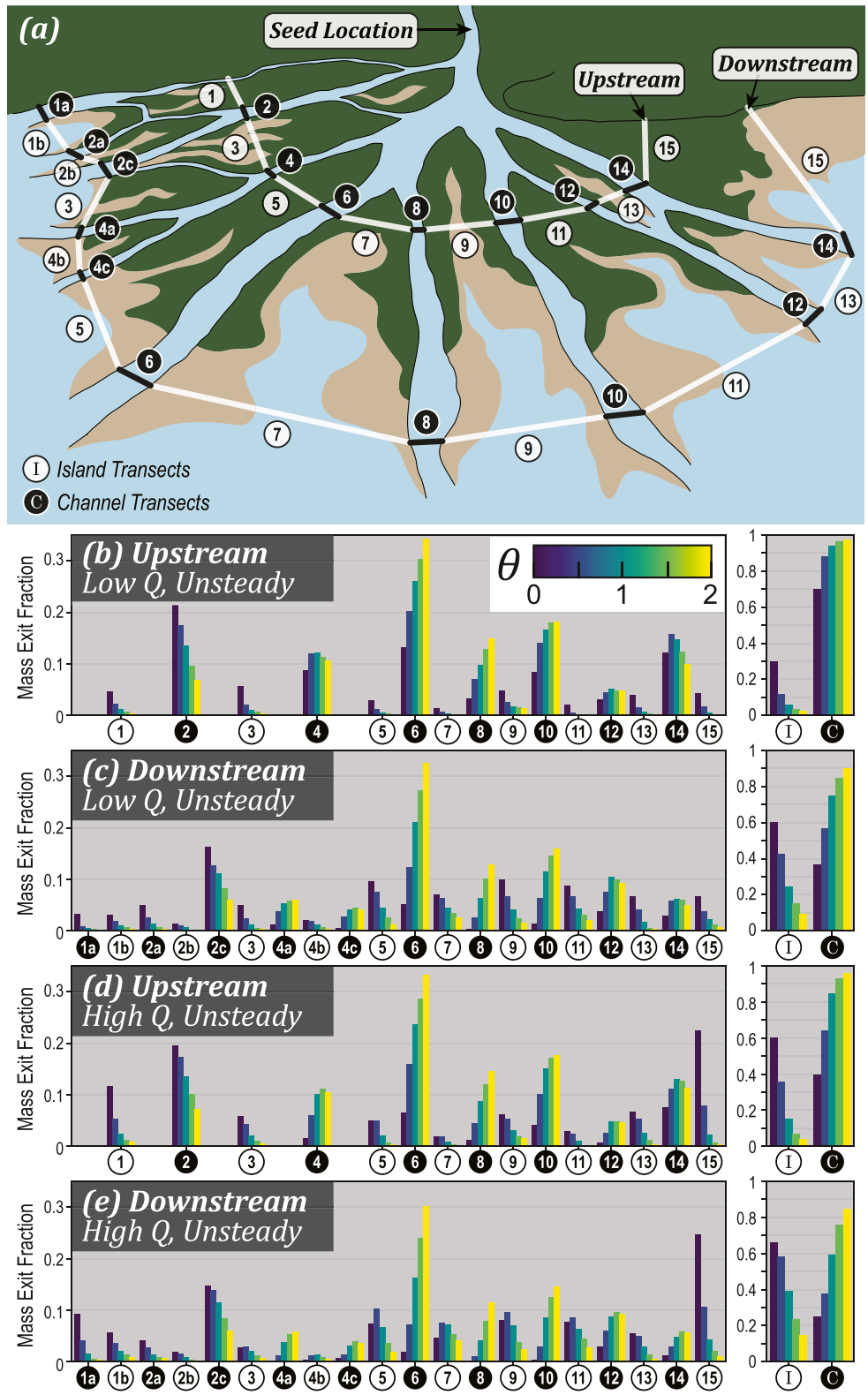

Figure 10. Quantification of connectivity at upstream and downstream transects in the Wax Lake Delta. (a) Locations and IDs for each transect, with channel transects shown in black and island transects shown in white (b–e) Fraction of particles which exited the domain out of each transect, as a function of θ (color), location (upstream (b, d) or downstream (c, e)), and discharge (Q_L (b, c) or Q_H (d, e)). Bulk island (I) and channel (C) fractions are shown on the right with an expanded y-axis.

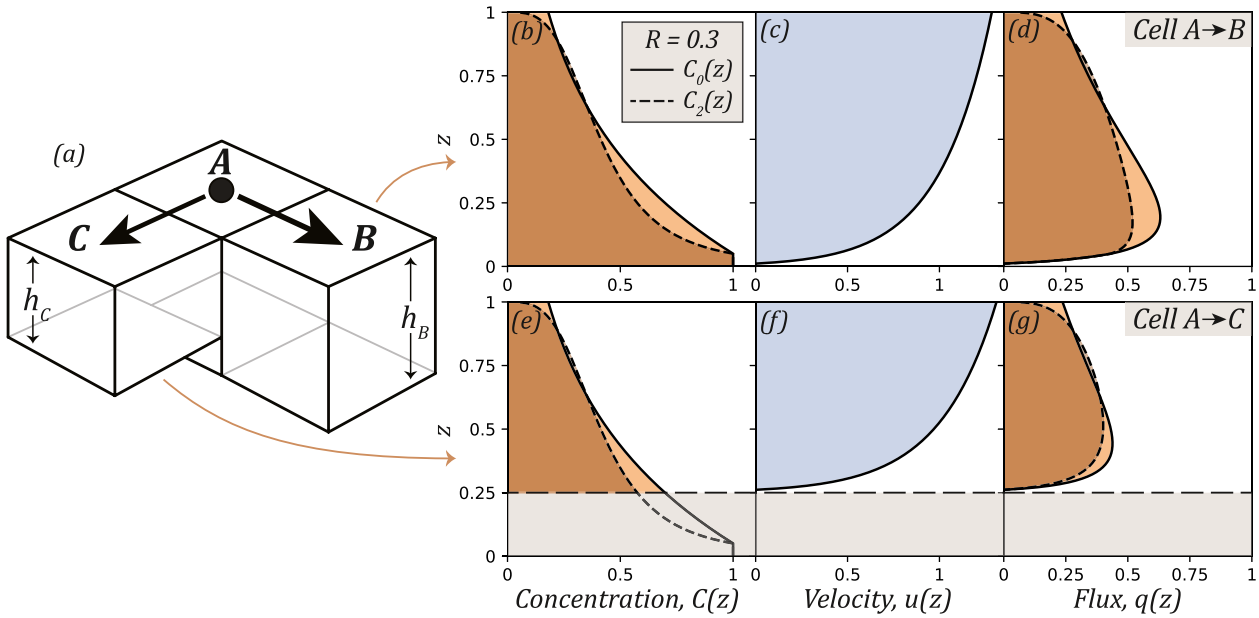

Figure 11. Framework of the conceptual model. (a) Schematic of the simplified three-cell scenario, in which $h_A = h_B > h_C$. (b) Vertical concentration profile in Cell A for a negatively buoyant material with an $R = 0.3$. (c) Flow velocity profile from cell A to B. (d) Mass flux of material from cell A to B. (e–g) The same as above, but integrated over a lesser depth to correspond to the flux from cell A to C The ratio of the shaded areas in (g and d) is used to compute a corresponding θ via Equation 8.

provide a means by which the degree of topographic steering, which is controlled by θ, can be connected to the Rouse number, R, for some given material.

Filling in the details for this model, we allow the concentration profile $C(z)$ in A to follow either the exponential (Equation 2) or power-law (Equation 3) form (Figures 11b and 11e). We set the starting depth $h_A = h_B = 1$ m, with some $h_C < 1$ m to enforce topographic steering. We also set the reference concentration C_a to unity, with a reference depth $a = 5$ cm. We assume the concentration below the reference depth $C(z \le a) = C_a$ based on data presented in De Leeuw et al. (2020). We allow R to be positive or negative to account for variations in particle buoyancy, but when $R < 0$, we apply the same rules regarding the reference concentration to the top 5 cm of the flow instead of the bottom. We compute the mass flux q_s into each cell as the product of the concentration and the water velocity $u(z)$ integrated from the bed up to the water surface as follows:

$$q_{s,i} = \int_{h_i}^{\eta} C(z) \cdot u_i(z)\, dz \tag{6}$$

For simplicity, we assume the velocity $u(z)$ follows a logarithmic profile over the full water depth (Lamb et al., 2008) using a roughness height $z_0 = 0.011$ m based on data presented in Shaw et al. (2013) and normalize the profile to yield a depth-averaged velocity of 1 m/s into each of the two receiving cells (Figures 11c and 11f). In order to conserve mass, we make the simplifying assumption that the remaining material in A which was not routed to cell C (the shaded area in Figure 11e) is split between cells B and C in proportion to the existing fluxes out of each cell (Figures 11d and 11g), which keeps the ratio of the two constant. In reality, this material could either (a) be routed to cell C by "compressing" the depth profile or (b) be fully diverted to cell B, so our assumption represents a middle ground between these two possible end-members. Finally, we assume that differences in the `dorado` routing weights between cells B and C are proportional to the ratio of mass flux entering each cell, $w_i \propto q_i$ (shaded areas in Figures 11d and 11g). Combining this with Equations 5 and 6, it follows that

$$\left(\frac{q_{s,C}}{q_{s,B}}\right) \propto \left(\frac{h_C}{h_B}\right)^{\theta} \tag{7}$$

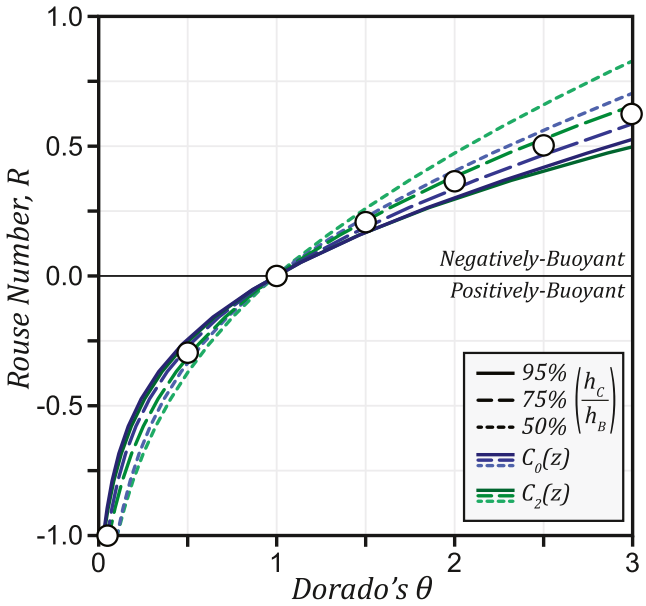

Figure 12. Estimated correspondence between the Rouse number, R, and `dorado`'s θ parameter. Each curve corresponds to some choice of Rouse profile and depth ratio, with reasonable global estimates of R for select θs indicated with white circles.

If we assume that the other terms in Equation 5 are approximately equal between cells B and C, we can rearrange this equation to solve for θ:

$$\theta \approx \frac{\ln(q_{s,C}) - \ln(q_{s,B})}{\ln(h_C)} \tag{8}$$

which we can compute numerically for a range of choices of R and h_C. By construction, this model enforces two key features described in less rigorous terms in Section 2.3: first, for materials entirely concentrated at the water surface, the mass flux into cells B and C will be equal regardless of depth and the numerator will cancel out, leading to a $\theta = 0$. This ensures that sufficiently buoyant materials will not have any sensitivity to topographic steering at the bottom of the water column. Second, for materials uniformly distributed throughout the water column, the mass flux into each cell will be exactly proportional to their respective depth, leading to an equal numerator and denominator and $\theta = 1$. This ensures that the routing of water is conservative.

Our conceptual model allows us to view the approximate correspondence between R and θ (Figure 12), shown here for three select values of $h_C \in [0.5, 0.75, 0.95]$. The model correctly reconstructs the intuitive process-level principles motivating θ—namely that decreases in buoyancy (i.e., increases in R) correspond to increases in θ. Both the exponential and power-law choices for $C(z)$ lead to a similar relationship between R and θ and largely overlap. Our three choices of h_C lead to slight differences in the resulting R-to-θ curve, although these differences tend to be small within the window of θs considered here and grow larger for increases in θ. The fact that these curves depend on h_C, which varies locally within the model domain, suggests that the accuracy of `dorado`/`DeltaRCM`'s simplified physics also varies slightly within the domain—however, the differences between these curves are small enough that we do not view this as a significant error, particularly within the range of θs considered herein. The vast majority of adjacent cells within our model domain differ only slightly in their depth (i.e., $h_C \approx h_B$), which means routing weights in these locations are already minimally dependent on θ. We expect topographic steering to matter most near channel margins, where the ratio of h_C/h_B tends to be the lowest, but is still virtually always ≥0.5. Reasonable global estimates of R for certain choices of θ are indicated in white circles (Figure 12), although it should be assumed that some variation exists around these values.

It follows from the relationship between R and θ (Figure 12) that the modeling results shown here all correspond to Rouse numbers $R \leq 0.5$. If we assign material types to our simulations based on field estimates, our highest $\theta = 2$ runs fall into the lower end of the $R \approx 0.3$–0.8 range for fine sands in suspension, and our second-highest $\theta = 1.5$ runs correspond to the $R \approx 0.1$–0.2 range for flocculated mud (Lamb et al., 2020). Water and other well-mixed materials in washload correspond to $\theta = 1$ as expected (Figure S1 in Supporting Information S1). Microplastics can theoretically occupy anywhere in this range but have primarily been found to fall into surface load ($\theta \approx 0$) or washload, with "rising suspended load" ($\theta \approx 0 - 0.5$) being a relatively rare transitionary domain (Cowger et al., 2021; Lenaker et al., 2019). We note that $\theta \geq 2$ is a reasonable approximation for sand, which is a common assumption in `DeltaRCM` that is supported by this conceptual model. Finally, because $\theta = 0$ is approached asymptotically and does not directly correspond to any one value of R, it is fair to assume that any sufficiently buoyant material (e.g., large wood and floating vegetation) can be modeled with this limiting case.

6. Discussion

6.1. Comparing the Wax and Atchafalaya

In general, our simulations showed much more variation in patterns of nourishment in the WLD (Figure 5) than the ATD (Figure 6). Because these two deltas are fed by nearly identical fluvial inputs, we hypothesize that these differences are largely the result of anthropogenic influence in the ATD. Significant amounts of dredging have created very different island and channel geometries in the ATD (Zhang et al., 2021), whereas the more shallow topographic gradients in WLD have been constructed almost entirely from natural processes (Paola et al., 2011).

This allows for increased connectivity and island nourishment in the WLD, and more radially uniform nourishment of the delta front by fluvial inputs. In the ATD, dredging in the dominant Southwest Pass appears to have preferentially diverted flows toward that distributary, particularly in sediment-like scenarios with $\theta \geq 1$ (Figures 6c, 6f, 6i and 6l). Our findings suggest that natural land-building processes in the WLD are more optimized for partitioning fluvial inputs evenly across the delta plain, resulting in more channel-island connectivity and increasing the land-building potential of each island.

6.2. The Role of Hydraulic Sorting

Our simulations clearly show that differences in local topographic steering can lead to a global reorganization of fluvial fluxes in river deltas. Even small changes to a local routing parameter θ led to emergent system-scale differences in patterns of nourishment and connectivity, as well as different sensitivities to changing environmental forcings. While this simplified framework leaves out a number of important physical processes that would influence transport, including deposition and entrainment in particular, it is clear from these simulations that vertical stratification combined with topographic steering on their own are sufficient to create large asymmetries in the partitioning of different kinds of materials, hydraulically segregating or sorting them into different regions of space.

In particular, the degree to which positively and negatively buoyant materials were sorted spatially can have important implications for the ecogeomorphic evolution of river deltas. Sediments and biotic materials (e.g., floating vegetation, seeds, and large wood) tend to concentrate in different portions of the water column (Figures 4 and 12), so this process implies that each of these materials have different characteristic pathways of transport in deltaic systems, leading to discrepancies in their deposits. While our "passive" simulations do not model deposition, these findings suggest that biotic materials could deposit in islands much farther upstream due to increases in channel-island connectivity experienced by surface flows. These differences could be further exacerbated (or alleviated) by differential entrainment (e.g., Enders et al., 2019) or granular sorting processes (Slingerland, 1984). Hydraulic sorting can therefore reinforce spatial gradients within the system between locations of sediment deposition, vegetation colonization, and fluxes of water, and these internal gradients drive deltaic processes like flow reorganization and island planform evolution.

In addition, because low-θ particle trajectories showed a greater sensitivity to changes in discharge and tides (Figures 8 and 9), these findings suggest a means by which external flows of energy into river deltas (from environmental forcings) can reinforce internal spatial gradients inside the system between different fluvial inputs. While we do not assess the role of wind or waves in the present study, it seems likely that these additional forcings would also most strongly influence the transport patterns of positively buoyant materials. Our findings also indicated that increases in connectivity associated with discharge and tides do not occur via the same pathways of transport (Figure 8a vs. Figure 9a), which would ultimately control the locations of deposits resulting from each forcing. These insights could have important implications for studies trying to assess the effects of external forcings on delta morphology (Galloway, 1975; Nienhuis et al., 2020).

All of this being said, one important caveat to note is that all nourishment estimates are normalized relative to the same total number of particles. However, different materials do not enter these deltas at the same rate—for example, the mass influx of water is several orders of magnitude higher than that of sediment. It is therefore important to emphasize that all nourishment comparisons shown here are *relative* rather than *absolute* (Figures 7–9), and that the corresponding "particle mass" for one particular simulation does not necessarily equal that of another. For comparisons between runs of different discharge (Figure 8), one could argue that because the total mass inflow rate in the Q_H scenario is about four times that of the Q_L scenario, then it may be appropriate to scale the magnitude of nourishment proportionally. Here, we have presented the results without this scaling, as we prefer not to make any a priori assumptions about the incoming mass of material, but it is important to be clear that a location having a greater relative nourishment in the Q_L scenario does not mean it receives a greater total mass of material than in the Q_H case. We repeated the nourishment comparisons (Figure 8) with the nourishment of the Q_H case scaled to be four times that of Q_L and found that virtually all locations in the domain receive an equal or greater absolute nourishment in the Q_H case (Figure S2 in Supporting Information S1), which is unsurprising. However, there are a few small regions around Sherman Island at which we did observe a greater absolute nourishment at low-discharge in select scenarios (Figure S2a in Supporting Information S1), with and without tides.

6.3. The Accuracy of Water as a Proxy

We observed several noteworthy differences between the transport of water-like particles and that of nonwater-like particles. Our findings could have important implications for field and remote-sensing applications attempting to quantify the transport of nonwater materials. Very few regions in either delta were maximally nourished by a choice of $\theta = 1$ (Figure 7), due to the propensity for other kinds of materials to concentrate in particular regions of the system. Similarly, bulk estimates of channel-island connectivity for nonwater materials were correlated with hydrological connectivity but often significantly different in magnitude (Figure 10). These findings suggest that future studies should be cautious when using water-based connectivity estimates as a proxy for other materials that are not neutrally buoyant or easily mixed by turbulence. Water-based measurements of partitioning and connectivity remain a good proxy for fine-grained material transported in washload, which aligns with observations from numerous studies (Allison et al., 2012; Sorourian et al., 2022), but may overestimate connectivity for suspended sand with concentrations highest near the bed (Mashriqui, 2003; Shaw et al., 2013) and flocculated mud (Lamb et al., 2020). Similarly, we should be cautious when using concentrations measured near the water surface as a proxy for the full water column, and be aware that such approaches may lead to a bias in depth-averaged estimates, which is in line with recommendations from prior studies (Cowger et al., 2021; Lenaker et al., 2019). Because most of the fluvial sediment input in WLD is fine material transported in washload (Olliver & Edmonds, 2021), surface estimates are likely fairly representative of the rest of the water column (e.g., Jensen et al., 2019; Salter et al., 2022), but perhaps not representative for coarser sandy inputs. Our findings may provide a framework by which hydrological measurements can be translated to other materials (Figure 12). Water flow measurements could be used to constrain hydrodynamic models, which can then be used in conjunction with `dorado` to approximate hydraulic sorting processes for nonwater materials. This approach is applicable to any sort of suspended material, even if the hydrodynamic solution itself is depth-averaged.

6.4. Limitations

As with any reduced-complexity modeling approach, there are a number of limitations worth addressing. While `dorado`'s underlying methodology is based on physics, it does not explicitly model many of the physical processes that would be present in more sophisticated full-physics advection-diffusion models, and our results therefore cannot account for the role of these additional processes on transport patterns. While this is undoubtedly a limitation of this analysis, we also view this as a strength because it allows us to more easily generalize across different materials and contexts. Aside from their reduced computational demand, one commonly regarded advantage of reduced-complexity models is their ability to reduce the number of complex lower-level processes being simulated—many of which may not be relevant to the emergent macroscopic phenomenon of interest—in order to isolate specific explanatory mechanisms for study (Murray, 2003, 2007). In this analysis, the phenomenological representation of hydraulic sorting built-in to the `dorado` framework allows us to study this mechanism in general across a wide range of possible materials, which would be very challenging if other material-specific transport processes were included.

Of the transport mechanisms neglected in our current analysis, we note two in particular that we expect to be important for additional study: (a) the role of deposition/reentrainment and (b) vertical flow structures neglected by depth-averaged models. Regarding the former, our passive particle routing cannot account for processes controlling deposition onto the bed, interception by vegetation, or the entrainment of material via erosion inside the domain. All of these processes would influence nourishment patterns because downstream locations cannot be nourished by material that has already been deposited upstream, and some regions may only be nourished by the internal reorganization of material. Prior studies have suggested potential mechanisms by which deposition can influence the phase lag of sediment transport with respect to tides that could influence partitioning between distributary channels (Wagner & Mohrig, 2019). Erosion inside the WLD is also known to be significant, both inside of distributary channels (Shaw & Mohrig, 2014; Whaling & Shaw, 2020) and on island platforms due to waves (Styles et al., 2021) or storms (Xing et al., 2017) but is not accounted for in our approach that only considers recent fluvial inputs. Future studies could use `dorado` or modifications thereof to investigate these processes, but they are not the focus of this study.

Regarding the latter, because the numerical solution from `ANUGA` is 2D, the model is unable to resolve the vertical component of hydrodynamics. This may be important near the channel-island interface, where recirculations can lead to an ostensibly 3D flow structure that could impact the flux of materials leaving the channels

(Chowdhury et al., 2022; Proust & Nikora, 2020). While this is a limitation of our approach, fully 3D models are very computationally expensive and challenging to implement and calibrate, particularly in a tidal system with regular wetting and drying, and usually these efforts do not lead to noteworthy improvements in model accuracy (Bates, 2022). Future work is needed to ascertain the role of vertical circulation on sorting and to constrain the accuracy of the simplified approach used here.

In addition to model uncertainties, the Rouse-Vanoni theory underlying our conceptual model should also be understood as a fairly idealized model for vertical stratification. There is also an interesting trade off between the accuracy of the conceptual model's assumption of depth profile truncation and the importance of θ on particle routing. In locations where $h_C/h_B \approx 1$, depth profile truncation is likely a poor assumption, as suspended material routed near the bed would simply bypass small changes in topography. However, these are also locations where θ does not have a significant influence on material routing, so the accuracy of this assumption is less important. In locations where $h_C/h_B < 1$, θ has a bigger impact on routing weights and the truncation assumption is more physically plausible. In a sense, this implies that the accuracy of the conceptual model is greater in the places where it is needed, and less accurate in places where topographic steering is already unimportant. However, more sophisticated theoretical approaches or field data could be used to better constrain the relationship between θ and real material properties.

6.5. Future Work

Insights from the present study could be useful to or improved upon by a number of future studies. Field-based, remote-sensing, and numerical modeling approaches could all be useful to constrain or validate the nourishment estimates provided here. Notably, the recent Delta-X field and remote-sensing campaign collected substantial amounts of data in the WLD and ATD that could be leveraged to build upon the findings of the present study (JPL, 2021), including in situ sediment concentrations and depth profiles, high-resolution hyperspectral and SAR imagery of the water surface (e.g., Jensen et al., 2019), and ample hydrological measurements to constrain water and sediment budgets in this landscape.

Our nourishment estimates can inform additional field research by suggesting locations where particular materials might accumulate. In particular, our findings suggest that the shoreline-adjacent islands of the WLD, which have often been neglected in prior studies, may be underrated with regards to their significance (Figures 5 and 10). Because `dorado` is open-source and can be used with any hydrodynamic model solution, a similar analysis could be repeated in other landscapes, for any fluvially transported material of interest. Due to the lack of a priori constraints on the kinds of materials that can be modeled using this framework, the implications of this study could be far-reaching and interdisciplinary.

Future work should aim to improve our theoretical understanding of sorting processes, and their influence on spatial patterns of nourishment in deltas and elsewhere. In particular, material properties and environmental conditions could have a very different influence on entrainment sorting (Slingerland, 1984) than on hydraulic sorting, and it would be interesting to see how these two sorting processes act in tandem to distribute material throughout deltaic systems. Results from more sophisticated morphodynamic or 3D models could be compared to our estimates of nourishment to better tease apart which transport processes are most important for landscape change.

7. Conclusions

In the present study, we utilized a mixed Eulerian-Lagrangian modeling framework to quantify patterns of material nourishment and connectivity in the Wax Lake and Atchafalaya deltas in coastal Louisiana. Our reduced-complexity particle routing approach allowed us to single out the influence of vertical stratification and topographic steering on the transport of a variety of fluvially transported materials, including water, sediments, biotic materials, and plastics, to name a few. Several key conclusions of this analysis are summarized as follows:

- Even small changes in local topographic steering, as controlled by `dorado`'s θ parameter, led to emergent system-scale changes in patterns of fluvial nourishment, with greater channel-island connectivity for positively buoyant materials than negatively buoyant materials, hydraulically sorting them in space.

- Nourishment patterns of low-θ particles were observed to be more sensitive to changes in tidal and discharge conditions than high-θ particles, suggesting a means by which external flows of energy into river deltas can reinforce spatial gradients between different kinds of materials.
- Differences in nourishment patterns between the WLD and ATD appear to be the result of anthropogenic dredging, suggesting that natural land building processes distribute materials more evenly across the delta plain.
- We utilized Rouse-Vanoni theory to construct a conceptual model to bridge the gap between material properties and the reduced-complexity approach of `dorado`/`DeltaRCM`, and that correspondence can be used to inform future applications of either model.
- We discussed how our nourishment and connectivity estimates tie together with prior research in these deltas and provide a means by which estimates of hydrological connectivity can be translated to other materials of interest.
- Our study provides a new modeling framework for studying material transport that could be readily applied to other systems or other materials and used to inform future field studies.

Data Availability Statement

All hydrodynamic outputs, `dorado` simulation results, and codes needed to reproduce this analysis are available for download at https://doi.org/10.5281/zenodo.7187585. Current links for the run-scripts of the `ANUGA` model of the Wax Lake and Atchafalaya Delta system can be found at deltax.jpl.nasa.gov and the final versions will be accessible via the ORNL DAAC. The particle-tracking model `dorado` is fully open-source and has been archived at https://doi.org/10.5281/zenodo.6454729, and the most up-to-date version can be found on GitHub at https://github.com/passaH2O/dorado.

Acknowledgments
This work was supported primarily by the NASA Delta-X project, which is funded by the Science Mission Directorate's Earth Science Division through the Earth Venture Suborbital-3 Program NNH17ZDA001N-EVS3. We also acknowledge partial support by the National Science Foundation via NSF EAR-1719670. We thank the Texas Advanced Computing Center (TACC) at the University of Texas at Austin for providing HPC resources that have contributed to the research results reported within this paper. We thank David Mohrig, Ben Hodges, Andrew Moodie, Nelson Tull, and Marc Simard for helpful feedback on this work. We also thank the rest of the Delta-X research team. Finally, we thank Editor Ton Hoitink and Associate Editor Christophe Ancey for handling this manuscript, as well as Brad Murray and one anonymous reviewer for peer-reviewing this work.

References

Allison, M. A., Demas, C. R., Ebersole, B. A., Kleiss, B. A., Little, C. D., Meselhe, E. A., et al. (2012). A water and sediment budget for the lower Mississippi–Atchafalaya River in flood years 2008–2010: Implications for sediment discharge to the oceans and coastal restoration in Louisiana. *Journal of Hydrology*, *432*, 84–97. https://doi.org/10.1016/j.jhydrol.2012.02.020

Amoros, C., & Bornette, G. (2002). Connectivity and biocomplexity in waterbodies of riverine floodplains. *Freshwater Biology*, *47*(4), 761–776. https://doi.org/10.1046/j.1365-2427.2002.00905.x

Atwood, E. C., Falcieri, F. M., Piehl, S., Bochow, M., Matthies, M., Franke, J., et al. (2019). Coastal accumulation of microplastic particles emitted from the Po River, Northern Italy: Comparing remote sensing and hydrodynamic modelling with in situ sample collections. *Marine Pollution Bulletin*, *138*, 561–574. https://doi.org/10.1016/j.marpolbul.2018.11.045

Ayoub, F., Jones, C., Lamb, M., Holt, B., Shaw, J., Mohrig, D., & Wagner, W. (2018). Inferring surface currents within submerged, vegetated deltaic islands and wetlands from multi-pass airborne SAR. *Remote Sensing of Environment*, *212*, 148–160. https://doi.org/10.1016/j.rse.2018.04.035

Baar, A., Boechat Albernaz, M., Van Dijk, W., & Kleinhans, M. (2019). Critical dependence of morphodynamic models of fluvial and tidal systems on empirical downslope sediment transport. *Nature Communications*, *10*(1), 1–12. https://doi.org/10.1038/s41467-019-12753-x

Bates, P. D. (2022). Flood inundation prediction. *Annual Review of Fluid Mechanics*, *54*(1), 287–315. https://doi.org/10.1146/annurev-fluid-030121-113138

Bevington, A. E., & Twilley, R. R. (2018). Island edge morphodynamics along a chronosequence in a prograding deltaic floodplain wetland. *Journal of Coastal Research*, *344*, 806–817. https://doi.org/10.2112/JCOASTRES-D-17-00074.1

Bouchez, J., Galy, V., Hilton, R. G., Gaillardet, J., Moreira-Turcq, P., Pérez, M. A., et al. (2014). Source, transport and fluxes of Amazon River particulate organic carbon: Insights from river sediment depth-profiles. *Geochimica et Cosmochimica Acta*, *133*, 280–298. https://doi.org/10.1016/j.gca.2014.02.032

Brush, J., & Lucien, M. (1965). Sediment sorting in Alluvial channels. In *Primary sedimentary structures and their hydrodynamic interpretation*. SEPM Society for Sedimentary Geology. https://doi.org/10.2110/pec.65.08.0025

Camenen, B., & Larson, M. (2008). A general formula for noncohesive suspended sediment transport. *Journal of Coastal Research*, *24*(3), 615–627. https://doi.org/10.2112/06-0694.1

Carle, M. V., Wang, L., & Sasser, C. E. (2014). Mapping freshwater marsh species distributions using WorldView-2 high-resolution multispectral satellite imagery. *International Journal of Remote Sensing*, *35*(13), 4698–4716. https://doi.org/10.1080/01431161.2014.919685

Cathcart, C., Shaw, J. B., & Amos, M. (2020). Validation of streaklines as recorders of synoptic flow direction in a deltaic setting. *Remote Sensing*, *12*(1), 148. https://doi.org/10.3390/rs12010148

Chambert, S., & James, C. (2009). Sorting of seeds by hydrochory. *River Research and Applications*, *25*(1), 48–61. https://doi.org/10.1002/rra.1093

Chowdhury, M. K., Konsoer, K. M., & Hiatt, M. (2022). Effect of lateral outflow on three-dimensional flow structure in a river delta. *Water Resources Research*, *58*(10), e2021WR031346. https://doi.org/10.1029/2021WR031346

Christensen, A., Twilley, R. R., Willson, C. S., & Castañeda-Moya, E. (2020). Simulating hydrological connectivity and water age within a coastal deltaic floodplain of the Mississippi River Delta. *Estuarine, Coastal and Shelf Science*, *245*, 106995. https://doi.org/10.1016/j.ecss.2020.106995

Couvillion, B. R., Beck, H., Schoolmaster, D., & Fischer, M. (2017). Land area change in coastal Louisiana from 1932 to 2016: U.S. Geological Survey scientific Investigations Map 3381, 16 p. pamphlet, Technical Report. U.S. Geological Survey. https://doi.org/10.3133/sim3381

Cowger, W., Gray, A. B., Guilinger, J. J., Fong, B., & Waldschlager, K. (2021). Concentration depth profiles of microplastic particles in river flow and implications for surface sampling. *Environmental Science and Technology*, *55*(9), 6032–6041. https://doi.org/10.1021/acs.est.1c01768

Dagestad, K.-F., Röhrs, J., Breivik, Ø., & Ådlandsvik, B. (2018). OpenDrift v1. 0: A generic framework for trajectory modelling. *Geoscientific Model Development*, *11*(4), 1405–1420. https://doi.org/10.5194/gmd-11-1405-2018

Davies, G., & Roberts, S. (2015). Open source flood simulation with a 2D discontinuous-elevation hydrodynamic model. In *Proceedings of MODSIM 2015*.

de Brye, B., Schellen, S., Sassi, M., Vermeulen, B., Kärnä, T., Deleersnijder, E., & Hoitink, T. (2011). Preliminary results of a finite-element, multi-scale model of the Mahakam Delta (Indonesia). *Ocean Dynamics*, *61*(8), 1107–1120. https://doi.org/10.1007/s10236-011-0410-y

De Laurentiis, L., Jones, C. E., Holt, B., Schiavon, G., & Del Frate, F. (2020). Deep learning for mineral and biogenic oil slick classification with airborne synthetic aperture radar data. *IEEE Transactions on Geoscience and Remote Sensing*, *59*(10), 8455–8469. https://doi.org/10.1109/TGRS.2020.3034722

De Leeuw, J., Lamb, M. P., Parker, G., Moodie, A. J., Haught, D., Venditti, J. G., & Nittrouer, J. A. (2020). Entrainment and suspension of sand and gravel. *Earth Surface Dynamics*, *8*(2), 485–504. https://doi.org/10.5194/esurf-8-485-2020

Denbina, M., Simard, M., Pavelsky, T., Christensen, A., Liu, K., & Lyon, C. (2020). Pre-Delta-X: Channel Bathymetry of the Atchafalaya Basin, LA, USA, 2016, ORNL DAAC. https://doi.org/10.3334/ORNLDAAC/1807

Dong, T. Y., Nittrouer, J. A., McElroy, B., Il'icheva, E., Pavlov, M., Ma, H., et al. (2020). Predicting water and sediment partitioning in a delta channel network under varying discharge conditions. *Water Resources Research*, *56*(11), e2020WR027199. https://doi.org/10.1029/2020WR027199

Doyle, M. W., & Ensign, S. H. (2009). Alternative reference frames in river system science. *BioScience*, *59*(6), 499–510. https://doi.org/10.1525/bio.2009.59.6.8

DuMars, A. J. (2002). *Distributary mouth bar formation and channel bifurcation in the Wax Lake Delta, Atchafalaya Bay, Louisiana, Master's thesis*. Louisiana State University. https://doi.org/10.31390/gradschool_theses.1856

Edmonds, D. A., Chadwick, A. J., Lamb, M. P., Lorenzo-Trueba, J., Murray, A. B., Nardin, W., et al. (2021). Morphodynamic modeling of river-dominated deltas: A review and future perspectives. In *Treatise on geomorphology*. Elsevier. https://doi.org/10.1016/B978-0-12-818234-5.00076-6

Edmonds, D. A., Paola, C., Hoyal, D. C., & Sheets, B. A. (2011). Quantitative metrics that describe river deltas and their channel networks. *Journal of Geophysical Research*, *116*(F4), F04022. https://doi.org/10.1029/2010JF001955

Edmonds, D. A., & Slingerland, R. L. (2008). Stability of delta distributary networks and their bifurcations. *Water Resources Research*, *44*(9). https://doi.org/10.1029/2008WR006992

Enders, K., Käppler, A., Biniasch, O., Feldens, P., Stollberg, N., Lange, X., et al. (2019). Tracing microplastics in aquatic environments based on sediment analogies. *Scientific Reports*, *9*(1), 1–15. https://doi.org/10.1038/s41598-019-50508-2

Esposito, C. R., Shen, Z., Törnqvist, T. E., Marshak, J., & White, C. (2017). Efficient retention of mud drives land building on the Mississippi Delta plain. *Earth Surface Dynamics*, *5*(3), 387–397. https://doi.org/10.5194/esurf-5-387-2017

Forbes, D., & Taylor, R. (1994). Ice in the shore zone and the geomorphology of cold coasts. *Progress in Physical Geography*, *18*(1), 59–89. https://doi.org/10.1177/030913339401800104

Galloway, W. E. (1975). Process framework for describing the morphologic and stratigraphic evolution of deltaic depositional systems. In *Deltas: Models for exploration* (pp. 87–98). Houston Geological Society.

Glenn, E. P., Zamora-Arroyo, F., Nagler, P. L., Briggs, M., Shaw, W., & Flessa, K. (2001). Ecology and conservation biology of the Colorado River delta, Mexico. *Journal of Arid Environments*, *49*(1), 5–15. https://doi.org/10.1006/jare.2001.0832

Han, J., & Kim, W. (2022). Linking levee-building processes with channel avulsion: Geomorphic analysis for assessing avulsion frequency and channel reoccupation. *Earth Surface Dynamics*, *10*(4), 743–759. https://doi.org/10.5194/esurf-10-743-2022

Hanegan, K., & Georgiou, I. (2015). Tidal modulated flow and sediment flux through wax lake delta distributary channels: Implications for delta development. *Proceedings of the International Association of Hydrological Sciences*, *367*, 391–398. https://doi.org/10.5194/piahs-367-391-2015

Hariharan, J., Wright, K., & Passalacqua, P. (2020). dorado: A Python package for simulating passive particle transport in shallow-water flows. *Journal of Open Source Software*, *5*(54), 2585. https://doi.org/10.21105/joss.02585

Hiatt, M. (2016). *Characterizing hydrological connectivity and channel-island processes in river deltas to inform coastal restoration. Ph.D. thesis*. The University of Texas at Austin. https://doi.org/10.15781/T2QZ23242

Hiatt, M., Castañeda-Moya, E., Twilley, R., Hodges, B. R., & Passalacqua, P. (2018). Channel-island connectivity affects water exposure time distributions in a coastal river delta. *Water Resources Research*, *54*, 2212–2232. https://doi.org/10.1002/2017WR021289

Hiatt, M., & Passalacqua, P. (2015). Hydrological connectivity in river deltas: The first-order importance of channel-island exchange. *Water Resources Research*, *51*(4), 2264–2282. https://doi.org/10.1002/2014WR016149

Hiatt, M., & Passalacqua, P. (2017). What controls the transition from confined to unconfined flow? Analysis of hydraulics in a coastal river delta. *Journal of Hydraulic Engineering*, *143*(6), 03117003. https://doi.org/10.1061/(ASCE)HY.1943-7900.0001309

Jensen, D., Simard, M., Cavanaugh, K., Sheng, Y., Fichot, C. G., Pavelsky, T., & Twilley, R. (2019). Improving the transferability of suspended solid estimation in wetland and deltaic waters with an empirical hyperspectral approach. *Remote Sensing*, *11*(13), 1629. https://doi.org/10.3390/rs11131629

JPL. (2021). The NASA Delta-X Project. Retrieved from https://deltax.jpl.nasa.gov/

Kane, I. A., & Clare, M. A. (2019). Dispersion, accumulation, and the ultimate fate of microplastics in deep-marine environments: A review and future directions. *Frontiers of Earth Science*, *7*, 80. https://doi.org/10.3389/feart.2019.00080

Kim, W., Mohrig, D., Twilley, R., Paola, C., & Parker, G. (2009). Is it feasible to build new land in the Mississippi River Delta? *EOS, Transactions American Geophysical Union*, *90*(42), 373–374. https://doi.org/10.1029/2009eo420001

Knights, D., Sawyer, A. H., Barnes, R. T., Piliouras, A., Schwenk, J., Edmonds, D. A., & Brown, A. M. (2020). Nitrate removal across ecogeomorphic zones in Wax Lake Delta, Louisiana (USA). *Water Resources Research*, *56*(8), e2019WR026867. https://doi.org/10.1029/2019WR026867

Kooi, M., Reisser, J., Slat, B., Ferrari, F. F., Schmid, M. S., Cunsolo, S., et al. (2016). The effect of particle properties on the depth profile of buoyant plastics in the ocean. *Scientific Reports*, *6*(1), 1–10. https://doi.org/10.1038/srep33882

Kukulka, T., Proskurowski, G., Morét-Ferguson, S., Meyer, D. W., & Law, K. L. (2012). The effect of wind mixing on the vertical distribution of buoyant plastic debris. *Geophysical Research Letters*, *39*(7), 7601. https://doi.org/10.1029/2012GL051116

Lamb, M. P., de Leeuw, J., Fischer, W. W., Moodie, A. J., Venditti, J. G., Nittrouer, J. A., et al. (2020). Mud in rivers transported as flocculated and suspended bed material. *Nature Geoscience*, *13*(8), 566–570. https://doi.org/10.1038/s41561-020-0602-5

Lamb, M. P., Dietrich, W. E., & Sklar, L. S. (2008). A model for fluvial bedrock incision by impacting suspended and bed load sediment. *Journal of Geophysical Research*, *113*(F3), F03025. https://doi.org/10.1029/2007JF000915

Lauzon, R., & Murray, A. B. (2018). Comparing the cohesive effects of mud and vegetation on delta evolution. *Geophysical Research Letters*, *45*(19), 10–437. https://doi.org/10.1029/2018GL079405

Lauzon, R., & Murray, A. B. (2022). Discharge determines avulsion regime in model experiments with vegetated and unvegetated deltas. *Journal of Geophysical Research: Earth Surface*, *127*(2), e2021JF006225. https://doi.org/10.1029/2021JF006225

Lauzon, R., Piliouras, A., & Rowland, J. C. (2019). Ice and permafrost effects on delta morphology and channel dynamics. *Geophysical Research Letters*, *46*(12), 6574–6582. https://doi.org/10.1029/2019GL082792

Lebreton, L., Van Der Zwet, J., Damsteeg, J.-W., Slat, B., Andrady, A., & Reisser, J. (2017). River plastic emissions to the world's oceans. *Nature Communications*, *8*(1), 1–10. https://doi.org/10.1038/ncomms15611

Le Lay, Y.-F., Piégay, H., & Moulin, B. (2013). Wood entrance, deposition, transfer and effects on fluvial forms and processes: Problem statements and challenging issues. *Treatise on geomorphology*, *12*, 20–36. https://doi.org/10.1016/B978-0-12-374739-6.00320-1

Lenaker, P. L., Baldwin, A. K., Corsi, S. R., Mason, S. A., Reneau, P. C., & Scott, J. W. (2019). Vertical distribution of microplastics in the water column and surficial sediment from the Milwaukee River Basin to Lake Michigan. *Environmental Science and Technology*, *53*(21), 12227–12237. https://doi.org/10.1021/acs.est.9b03850

Liang, M., Geleynse, N., Edmonds, D., & Passalacqua, P. (2015). A reduced-complexity model for river delta formation–Part 2: Assessment of the flow routing scheme. *Earth Surface Dynamics*, *3*(1), 87–104. https://doi.org/10.5194/esurf-3-87-2015

Liang, M., Kim, W., & Passalacqua, P. (2016). How much subsidence is enough to change the morphology of river deltas? *Geophysical Research Letters*, *43*(19), 10–266. https://doi.org/10.1002/2016GL070519

Liang, M., Van Dyk, C., & Passalacqua, P. (2016). Quantifying the patterns and dynamics of river deltas under conditions of steady forcing and relative sea level rise. *Journal of Geophysical Research: Earth Surface*, *121*(2), 465–496. https://doi.org/10.1002/2015JF003653

Liang, M., Voller, V., & Paola, C. (2015). A reduced-complexity model for river delta formation–Part 1: Modeling deltas with channel dynamics. *Earth Surface Dynamics*, *3*(1), 67–86. https://doi.org/10.5194/esurf-3-67-2015

Ma, H., Larsen, L. G., & Wagner, R. W. (2018). Ecogeomorphic feedbacks that grow deltas. *Journal of Geophysical Research: Earth Surface*, *123*(12), 3228–3250. https://doi.org/10.1029/2018JF004706

Mashriqui, H. S. (2003). *Hydrodynamic and sediment transport modeling of deltaic sediment processes, Ph.D. thesis*. Louisiana State University. https://doi.org/10.31390/gradschool_dissertations.1483

Mazzorana, B., Hübl, J., Zischg, A., & Largiader, A. (2011). Modelling woody material transport and deposition in alpine rivers. *Natural Hazards*, *56*(2), 425–449. https://doi.org/10.1007/s11069-009-9492-y

Messyasz, B., Pikosz, M., & Treska, E. (2018). *Biology of freshwater Macroalgae and their Distribution* (pp. 17–31). Springer International Publishing. https://doi.org/10.1007/978-3-319-74703-3_3

Moodie, A. J., Hariharan, J., Barefoot, E., & Passalacqua, P. (2021). pyDeltaRCM: A flexible numerical delta model. *Journal of Open Source Software*, *6*(64), 3398. https://doi.org/10.21105/joss.03398

Moodie, A. J., & Passalacqua, P. (2021). When does faulting-induced subsidence drive distributary network reorganization? *Geophysical Research Letters*, *48*(22), e2021GL095053. https://doi.org/10.1029/2021GL095053

Mungkasi, S., & Roberts, S. (2013). Validation of ANUGA hydraulic model using exact solutions to shallow water wave problems. *Journal of Physics: Conference Series*, *423*, 012029. https://doi.org/10.1088/1742-6596/423/1/012029

Murray, A. B. (2003). Contrasting the goals, strategies, and predictions associated with simplified numerical models and detailed simulations. In *Prediction in geomorphology* (pp. 151–165). American Geophysical Union (AGU). chap. 11. https://doi.org/10.1029/135GM11

Murray, A. B. (2007). Reducing model complexity for explanation and prediction. *Geomorphology*, *90*(3), 178–191. https://doi.org/10.1016/j.geomorph.2006.10.020

Murray, A. B., & Paola, C. (2003). Modelling the effect of vegetation on channel pattern in bedload rivers. *Earth Surface Processes and Landforms*, *28*(2), 131–143. https://doi.org/10.1002/esp.428

Nielsen, O., Roberts, S., Gray, D., McPherson, A., & Hitchman, A. (2005). *Hydrodynamic modelling of coastal inundation*. Modelling and Simulation Society of Australia and New Zealand Inc.

Nienhuis, J. H., Ashton, A. D., Edmonds, D. A., Hoitink, A., Kettner, A. J., Rowland, J. C., & Törnqvist, T. (2020). Global-scale human impact on delta morphology has led to net land area gain. *Nature*, *577*(7791), 514–518. https://doi.org/10.1038/s41586-019-1905-9

O'Callaghan, J. F., & Mark, D. M. (1984). The extraction of drainage networks from digital elevation data. *Computer Vision, Graphics, and Image Processing*, *28*(3), 323–344. https://doi.org/10.1016/S0734-189X(84)80011-0

Olliver, E., & Edmonds, D. (2021). Hydrological connectivity controls magnitude and distribution of sediment deposition within the deltaic islands of Wax Lake Delta, LA, USA. *Journal of Geophysical Research: Earth Surface*, *126*(9), e2021JF006136. https://doi.org/10.1029/2021JF006136

Olliver, E. A., Edmonds, D., & Shaw, J. B. (2020). Influence of floods, tides, and vegetation on sediment retention in Wax Lake Delta, Louisiana, USA. *Journal of Geophysical Research: Earth Surface*, *125*(1), e2019JF005316. https://doi.org/10.1029/2019JF005316

Paola, C., Twilley, R. R., Edmonds, D. A., Kim, W., Mohrig, D., Parker, G., et al. (2011). Natural processes in delta restoration: Application to the Mississippi Delta. *Annual Review of Marine Science*, *3*(1), 67–91. https://doi.org/10.1146/annurev-marine-120709-142856

Pearson, K. (1905). The problem of the random walk. *Nature*, *72*(1867), 342. https://doi.org/10.1038/072294b0

Persi, E., Petaccia, G., Sibilla, S., Brufau, P., & García-Navarro, P. (2019). Calibration of a dynamic Eulerian-Lagrangian model for the computation of wood cylinders transport in shallow water flow. *Journal of Hydroinformatics*, *21*(1), 164–179. https://doi.org/10.2166/hydro.2018.085

Piliouras, A., Lauzon, R., & Rowland, J. C. (2021). Unraveling the combined effects of ice and permafrost on arctic delta morphodynamics. *Journal of Geophysical Research: Earth Surface*, *126*(4), e2020JF005706. https://doi.org/10.1029/2020JF005706

Proust, S., & Nikora, V. I. (2020). Compound open-channel flows: Effects of transverse currents on the flow structure. *Journal of Fluid Mechanics*, *885*, A24. https://doi.org/10.1017/jfm.2019.973

Reed, M., Turner, C., & Odulo, A. (1994). The role of wind and emulsification in modelling oil spill and surface drifter trajectories. *Spill Science & Technology Bulletin*, *1*(2), 143–157. https://doi.org/10.1016/1353-2561(94)90022-1

Repasch, M., Scheingross, J. S., Hovius, N., Vieth-Hillebrand, A., Mueller, C. W., Höschen, C., et al. (2022). River organic carbon fluxes modulated by hydrodynamic sorting of particulate organic matter. *Geophysical Research Letters*, *49*(3), e2021GL096343. https://doi.org/10.1029/2021GL096343

Roberts, H., Coleman, J., Bentley, S., & Walker, N. (2003). An embryonic major delta lobe: A new generation of delta studies in the Atchafalaya-Wax Lake Delta system. *Gulf Coast Association of Geological Societies Transactions*, *53*, 690–703.

Roberts, S., Nielsen, O., Gray, D., Sexton, J., & Davies, G. (2015). ANUGA User Manual, Geoscience Australia.

Röhrs, J., Dagestad, K.-F., Asbjørnsen, H., Nordam, T., Skancke, J., Jones, C. E., & Brekke, C. (2018). The effect of vertical mixing on the horizontal drift of oil spills. *Ocean Science*, *14*(6), 1581–1601. https://doi.org/10.5194/os-14-1581-2018

Rouse, H. (1937). Modern conceptions of the mechanics of fluid turbulence. *Transactions of the American Society of Civil Engineers*, *102*(1), 463–505. https://doi.org/10.1061/TACEAT.0004872

Salter, G., Passalacqua, P., Wright, K., Feil, S., Jensen, D., Simard, M., & Lamb, M. P. (2022). Spatial patterns of deltaic deposition/erosion revealed by streaklines extracted from remotely-sensed suspended sediment concentration. *Geophysical Research Letters*, *49*(11), e2022GL098443. https://doi.org/10.1029/2022GL098443

Sassi, M. G., Hoitink, A., De Brye, B., Vermeulen, B., & Deleersnijder, E. (2011). Tidal impact on the division of river discharge over distributary channels in the Mahakam Delta. *Ocean Dynamics*, *61*(12), 2211–2228. https://doi.org/10.1007/s10236-011-0473-9

Shaw, J. B., Estep, J. D., Whaling, A. R., Sanks, K. M., & Edmonds, D. A. (2018). Measuring subaqueous progradation of the Wax Lake Delta with a model of flow direction divergence. *Earth Surface Dynamics*, *6*(4), 1155–1168. https://doi.org/10.5194/esurf-6-1155-2018

Shaw, J. B., & Mohrig, D. (2014). The importance of erosion in distributary channel network growth, Wax Lake Delta, Louisiana, USA. *Geology*, *42*(1), 31–34. https://doi.org/10.1130/G34751.1

Shaw, J. B., Mohrig, D., & Wagner, R. W. (2016). Flow patterns and morphology of a prograding river delta. *Journal of Geophysical Research: Earth Surface*, *121*(2), 372–391. https://doi.org/10.1002/2015JF003570

Shaw, J. B., Mohrig, D., & Whitman, S. K. (2013). The morphology and evolution of channels on the Wax Lake Delta, Louisiana, USA. *Journal of Geophysical Research: Earth Surface*, *118*(3), 1562–1584. https://doi.org/10.1002/jgrf.20123

Shields, M. R., Bianchi, T. S., Mohrig, D., Hutchings, J. A., Kenney, W. F., Kolker, A. S., & Curtis, J. H. (2017). Carbon storage in the Mississippi River delta enhanced by environmental engineering. *Nature Geoscience*, *10*(11), 846–851. https://doi.org/10.1038/NGEO3044

Slingerland, R. (1984). Role of hydraulic sorting in the origin of fluvial placers. *Journal of Sedimentary Research*, *54*(1), 137–150. https://doi.org/10.1306/212F83C8-2B24-11D7-8648000102C1865D

Slingerland, R., & Smith, N. D. (1998). Necessary conditions for a meandering-river avulsion. *Geology*, *26*(5), 435–438. https://doi.org/10.1130/0091-7613(1998)026

Sorourian, S., Huang, H., Xu, K., Justic, D., & D'Sa, E. J. (2022). A modeling study of water and sediment flux partitioning through the major passes of Mississippi Birdfoot Delta and their plume structures. *Geomorphology*, *401*, 108109. https://doi.org/10.1016/j.geomorph.2022.108109

Styles, R., Snedden, G. A., Smith, S. J., Bryant, D. B., Boyd, B. M., Gailani, J. Z., et al. (2021). Seasonal controls on sediment delivery and hydrodynamics in a vegetated tidally influenced interdistributary island. *Journal of Geophysical Research: Oceans*, *126*(7), e2020JC016146. https://doi.org/10.1029/2020JC016146

Sundby, S. (1983). A one-dimensional model for the vertical distribution of pelagic fish eggs in the mixed layer. *Deep-Sea Research, Part A: Oceanographic Research Papers*, *30*(6), 645–661. https://doi.org/10.1016/0198-0149(83)90042-0

Svensson, U., & Omstedt, A. (1998). Numerical simulations of frazil ice dynamics in the upper layers of the ocean. *Cold Regions Science and Technology*, *28*(1), 29–44. https://doi.org/10.1016/S0165-232X(98)00011-1

Swarzenski, C. M. (2003). *Surface-water hydrology of the Gulf Intracoastal Waterway in South-Central Louisiana, 1996-99, Technical Report*. US Department of the Interior, US Geological Survey.

Thiel, M., & Gutow, L. (2004). The ecology of rafting in the marine environment. I. The floating substrata. *Oceanography and Marine Biology an Annual Review*, *42*, 181–264.

Thiel, M., & Gutow, L. (2005). The ecology of rafting in the marine environment. II. The rafting organisms and community. In *Oceanography and marine biology: An annual review* (pp. 289–428). CRC Press.

Torres, M. A., Kemeny, P. C., Lamb, M. P., Cole, T. L., & Fischer, W. W. (2020). Long-term storage and age-biased export of fluvial organic carbon: Field evidence from west Iceland. *Geochemistry, Geophysics, Geosystems*, *21*(4), e2019GC008632. https://doi.org/10.1029/2019GC008632

Tull, N., Passalacqua, P., Hassenruck-Gudipati, H. J., Rahman, S., Wright, K., Hariharan, J., & Mohrig, D. (2022). Bidirectional river-floodplain connectivity during combined pluvial-fluvial events. *Water Resources Research*, *58*(3), e2021WR030492. https://doi.org/10.1029/2021WR030492

Vanoni, V. A. (1946). Transportation of suspended sediment by water. *Transactions of the American Society of Civil Engineers*, *111*(1), 67–102. https://doi.org/10.1061/TACEAT.0005975

Van Rijn, L. C. (1993). *Principles of sediment transport in rivers, estuaries and coastal seas* (Vol. 1006). Aqua Publications.

Van Sebille, E., Aliani, S., Law, K. L., Maximenko, N., Alsina, J. M., Bagaev, A., et al. (2020). The physical oceanography of the transport of floating marine debris. *Environmental Research Letters*, *15*(2), 023003. https://doi.org/10.1088/1748-9326/ab6d7d

Wagner, W., Lague, D., Mohrig, D., Passalacqua, P., Shaw, J., & Moffett, K. (2017). Elevation change and stability on a prograding delta. *Geophysical Research Letters*, *44*(4), 1786–1794. https://doi.org/10.1002/2016GL072070

Wagner, W., & Mohrig, D. (2019). Flow and sediment flux asymmetry in a branching channel delta. *Water Resources Research*, *55*(11), 9563–9577. https://doi.org/10.1029/2019WR026050

Waldschläger, K., Brückner, M. Z., Almroth, B. C., Hackney, C. R., Adyel, T. M., Alimi, O. S., et al. (2022). Learning from natural sediments to tackle microplastics challenges: A multidisciplinary perspective. *Earth-Science Reviews*, *228*, 104021. https://doi.org/10.1016/j.earscirev.2022.104021

Walker, N. D., & Hammack, A. B. (2000). Impacts of winter storms on circulation and sediment transport: Atchafalaya-Vermilion Bay region, Louisiana, USA. *Journal of Coastal Research*, 996–1010.

Whaling, A., & Shaw, J. (2020). Changes to subaqueous delta bathymetry following a high river flow event, Wax Lake Delta, USA. *Estuaries and Coasts*, *43*(8), 1923–1938. https://doi.org/10.1007/s12237-020-00727-y

Wohl, E. (2013). Floodplains and wood. *Earth-Science Reviews*, *123*, 194–212. https://doi.org/10.1016/j.earscirev.2013.04.009

Wohl, E., Brierley, G., Cadol, D., Coulthard, T. J., Covino, T., Fryirs, K. A., et al. (2019). Connectivity as an emergent property of geomorphic systems. *Earth Surface Processes and Landforms*, *44*(1), 4–26. https://doi.org/10.1002/esp.4434

Wright, K., Hiatt, M., & Passalacqua, P. (2018). Hydrological connectivity in vegetated river deltas: The importance of patchiness below a threshold. *Geophysical Research Letters*, *45*(19), 10–416. https://doi.org/10.1029/2018GL079183

Wright, K., Passalacqua, P., Simard, M., & Jones, C. E. (2022). Integrating connectivity into hydrodynamic models: An automated open-source method to refine an unstructured mesh using remote sensing. *Journal of Advances in Modeling Earth Systems*, *14*(8), e2022MS003025. https://doi.org/10.1029/2022MS003025

Xing, F., Syvitski, J., Kettner, A., Meselhe, E., Atkinson, J., & Khadka, A. (2017). Morphological responses of the Wax Lake Delta, Louisiana, to Hurricanes Rita. *Elementa Science of the Anthropocene*, *5*, 80. https://doi.org/10.1525/elementa.125

Zhang, X., Xu, K., Yang, Z., Tan, X., & Wu, C. (2021). Decreasing land growth and unique seasonal area fluctuations of two newborn Mississippi subdeltas. *Geomorphology*, *378*, 107617. https://doi.org/10.1016/j.geomorph.2021.107617